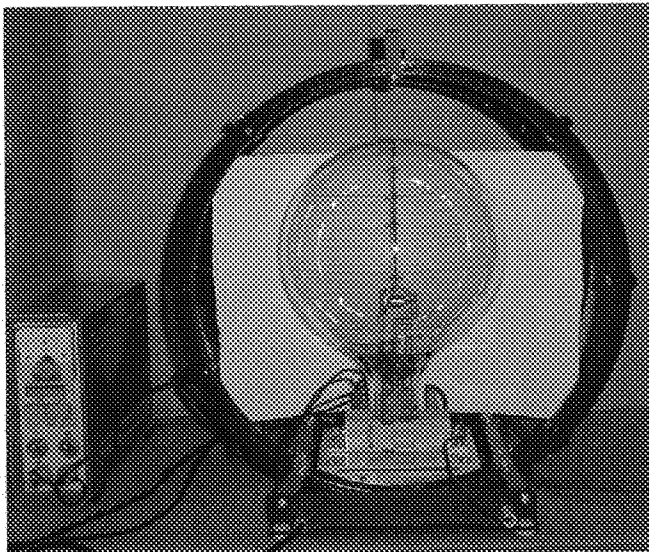


6.1. Electron	361
Thomson's discovery. Electron trajectory in transverse magnetic field. What is worth remembering. Shot-noise measurements of the electron charge.	
6.2. Michelson interferometer	371
Michelson's interferometer. Determination of the light wavelength. Refraction index of air. Refraction index of glass. Doppler effect.	
6.3. Principles of radio	379
Modulation and demodulation. Experimental setup. Calibration of the receiver. Selectivity of antenna circuit. Panorama of accessible broadcasting stations. Directivity diagram of antenna.	
6.4. Photoelectric effect	389
Planck's constant, Einstein's equation, and Millikan's experiment. Determination of the ratio h/e . The work function.	
6.5. Franck–Hertz experiment	397
Experiment and results. The excitation and ionization potentials.	
6.6. Thermionic emission	403
What is worth remembering. Richardson's method. Temperature of emitted electrons. Calorimetric determination of the work function.	
6.7. Transistor	418
Bipolar junction transistors. Junction field-effect transistors. Transistor amplifier.	
6.8. Superconductivity	425
Basic features of superconductors. High-temperature superconductivity. Resistance versus temperature. $U-I$ characteristic and critical current. Magnetization curves. Magnetic susceptibility versus external magnetic field. Transition curve. Diamagnetism of superconductors.	

6.1. Electron

The e/m ratio for the electron is calculated from measurements of the electron trajectory in a magnetic field. Shot-noise measurements are used for a determination of the electron charge (Kraftmakher 1995, 2005g). The charge and the mass of the electron are thus obtainable.



The Bainbridge tube used for determining the e/m ratio.

Additional equipment:

Two *Voltage sensors*, DC supplies, e/m apparatus, vacuum phototube, function generator, RMS/DC converter.



© The Nobel Foundation
Joseph John Thomson
(1856–1940)

"...You have thus been worthily treading in the footsteps of your great and renowned compatriots, Faraday and Maxwell, men who set to the world of science the highest and noblest examples."

J. P. Klason, President of the Royal Swedish Academy of Sciences. Presentation of Joseph John Thomson awarded the Nobel Prize "in recognition of the great merit of his theoretical and experimental investigations on the conduction of electricity by gases" (1906).

Thomson's discovery

The determination of fundamental physical constants remains an attractive goal of student experiments. The charge and mass of the electron are such fundamental constants. Joseph John Thomson discovered the electron in 1897. In his cathode tube, electrons were accelerated and then subjected to electric and magnetic fields, E and B . The Lorentz force F applied to a moving electron is

$$F = eE + ev \times B, \quad (1)$$

where e is the electron charge, and v is its velocity. The fields E and B were set to be perpendicular to each other and to the vector v . The forces eE and $ev \times B$ were directed in opposition, and it was possible to balance their actions. Under compensation,

$$v = E/B. \quad (2)$$

On the other hand, the velocity of the electrons can be calculated from the accelerating voltage U :

$$v = (2eU/m)^{1/2}, \quad (3)$$

where m is the mass of the electron. Hence,

$$e/m = E^2/2UB^2. \quad (4)$$

With the velocity known from Eq. (2), the e/m ratio for the electrons can also be found from measurements of their deflection by an electric field. Such a process occurs in a cathode-ray tube of an oscilloscope. In experiments involving the movement of electrons in electric and magnetic fields, the forces acting on the electron are proportional to its charge e , while the acceleration is inversely proportional to its mass m . This is the reason why only the e/m ratio is available from such measurements. Many methods, including very ingenious ones, exist for the determination of the e/m ratio. At the same time, the number of techniques for the determination of the electron charge is very limited. The main methods are the famous Millikan experiment with small oil drops and shot-noise measurements.

Glascock and Sparlin (1972) described an e/m experiment with a cathode-ray tube. Huggins and Lelek (1979) presented a series of laboratory experiments and computer simulations of the motion of electrons in electric and magnetic fields. Peterson (1983) designed various accessories for a commercially available e/m apparatus, the Bainbridge tube. Thompson (1990) proposed taking into account the Earth's magnetic field for more accurate determinations of the e/m ratio with the Bainbridge tube. To determine the e/m ratio, Yang (1998) used a magnetic focusing method. Rechenberg (1997) presented a chronology of discoveries related to the electron during 100 years.

Electron trajectory in transverse magnetic field

The Bainbridge tube for determining the e/m ratio (Fig. 1) is a more convenient apparatus than that used by Thomson. In a sealed chamber, a hot cathode emits electrons, which are accelerated by an electric field and focused into a beam. The electrons move in a region of uniform magnetic field produced by Helmholtz coils and directed perpendicular to their velocity. The magnetic force $ev \times \mathbf{B}$ continually deflects the electrons, causing them to follow a circular path. The path becomes

visible because atoms of a gas at low pressure in the chamber emit light when some of the electrons collide with them. From Newton's second law,

$$F = evB = mv^2/r, \quad \text{so that} \quad (5)$$

$$e/m = v/Br, \quad (6)$$

where r is the radius of the electron trajectory in the magnetic field. On the other hand, the velocity of the electrons depends on the accelerating voltage U :

$$v^2 = 2eU/m. \quad (7)$$

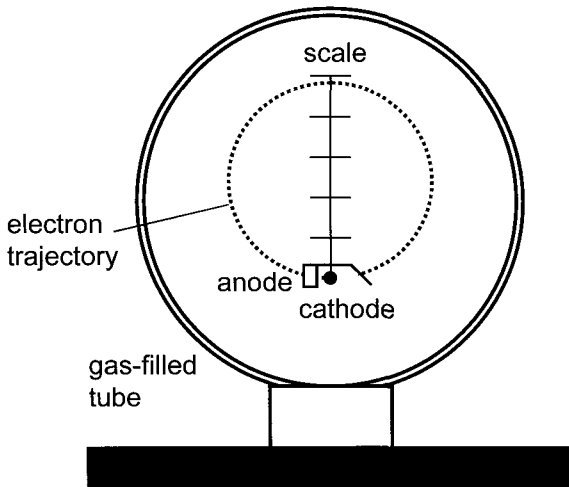


Fig. 1. Apparatus for determining the e/m ratio. Helmholtz coils producing the magnetic field perpendicular to the electron trajectory are not shown.

From the above equations, one obtains the e/m ratio:

$$e/m = 2U/B^2r^2. \quad (8)$$

For accurately determining the radius of the electron trajectory, a scale is arranged inside the chamber. The distance between two neighbouring marks equals 2 cm, and the maximum diameter of the trajectory is 10 cm. Two power supplies provide voltages for accelerating the emitted electrons (150 or 200 V) and heating the cathode (5 V). Since the second voltage amounts to several per cent of the accelerating voltage, it becomes important, to which side of the cathode

the anode circuit is connected. The best way is to connect it to a middle point between two similar resistors shunting the cathode (Fig. 2).

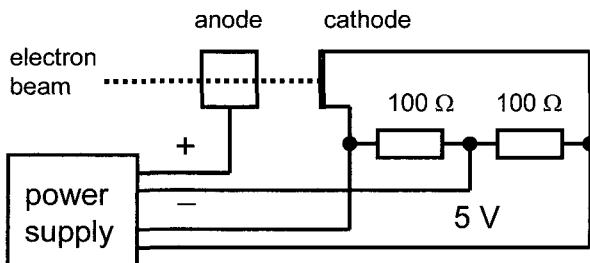


Fig. 2. The connection of the anode circuit to the cathode.

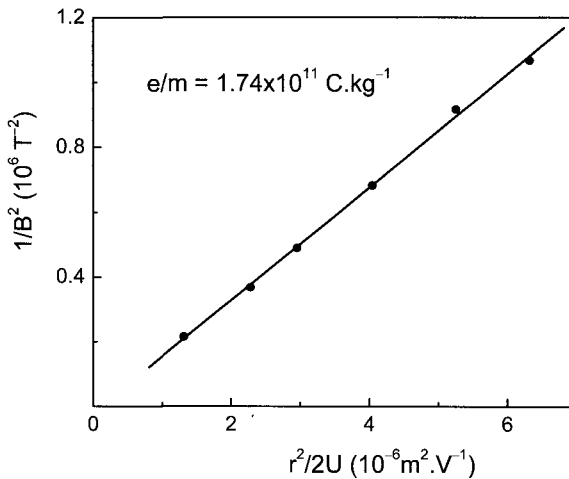


Fig. 3. The quantity $1/B^2$ versus $r^2/2U$.

The radius of the Helmholtz coils equals 0.15 m, and the number of turns is $N = 124$, so $B \text{ (T)} = 7.43 \times 10^{-4} \times I \text{ (A)}$. Another power supply provides a DC current for the Helmholtz coils. The e/m ratio is taken as the slope of a graph of $1/B^2$ versus $r^2/2U$ (Fig. 3). The error of the results obtained does not exceed 5%.

What is worth remembering

To avoid the influence of the Earth's magnetic field, the axis of the Helmholtz coils should be oriented perpendicular to the magnetic meridian. Otherwise, the horizontal component of the Earth's magnetic

field must be determined and taken into account. The simplest way of doing so is to observe, with a sufficiently low accelerating voltage, the electron trajectory with no current in the Helmholtz coils. If the electron trajectory is nearly perpendicular to the Earth's magnetic field, it is easy to see its curvature. Then one adjusts the current in the Helmholtz coils to straighten out the trajectory. This current should be added to (or subtracted from) all the currents necessary to achieve circular trajectories of definite radii. This is a useful additional exercise for students.

Shot-noise measurements of the electron charge

Along with the well-known Millikan experiment, the measurement of shot noise is an effective approach for the determination of the electron charge. Several papers have been published on the subject (Earl 1966; Livesey and McLeod 1973; Spiegel and Helmer 1995; Kraftmakher 1961, 1995, 2005g). Our experiment employs a vacuum phototube similarly to some other experiments (Portis 1964; Portis and Young 1971; Spiegel and Helmer 1995). The mean square of the fluctuations of the current is given by (e.g., Bleaney and Bleaney 1968)

$$\langle \Delta I^2 \rangle = 2eI\Delta f, \quad (9)$$

where e is the electron charge, I is the mean phototube current, and Δf is the frequency bandwidth, over which the noise is measured. When the current flows through a load of impedance Z , the mean square of the noise voltage across the load equals

$$\langle V^2 \rangle = 2eI \int_0^\infty |Z(f)|^2 df. \quad (10)$$

In our case, a parallel *LCR* circuit is the load of an illuminated vacuum phototube (Fig. 4). An advantage of this circuit is that it has low impedance for DC current and high impedance for fluctuations of the current at frequencies close to the resonance. As a source of the current, the phototube is connected in series with the *LCR* circuit. At the same time, the phototube is connected parallel to it, through a DC supply. The internal resistance of the phototube thus shunts the parallel *LCR* circuit and should be taken into account. The impedance of an *LCR* circuit can be expressed through its resonance angular frequency $\omega_0 = 2\pi f_0$ and the quality factor (*Q*-factor), which equals $Q = \omega_0 L / R$. Assuming $Q \gg 1$ and performing the integration in Eq. (10), one obtains a simple relation (Stigmark 1952; Kraftmakher 1961, 1995; Soloukhin 1975; Goldin 1983; Pippard 1989):

$$\langle V^2 \rangle = eIQ/2\omega_0 C^2. \quad (11)$$

With Eq. (11), one has no need for determining the frequency dependence of the impedance. Stigmark (1952) used this method for a precise determination of the electron charge. In our setup, three resistors are added to the basic circuit. The resistor R_1 serves for the determination of the mean photoelectric current. The resistor R_2 is connected through the resistor R_3 to a function generator. An AC voltage drop across the resistor R_2 drives forced oscillations in the LCR circuit. Relative to this voltage source, the elements of the LCR circuit are put in series. The forced oscillations serve to determine the Q -factor of the circuit. A DC supply provides a voltage for the phototube. Its output terminals should not be grounded.

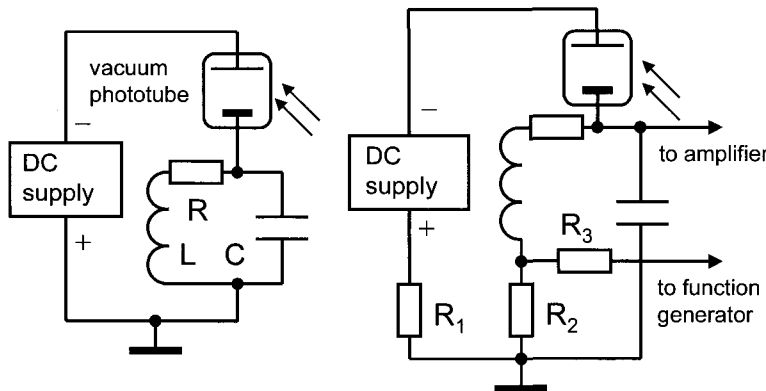


Fig. 4. Basic diagram of a vacuum phototube loaded by a parallel LCR circuit, and diagram showing additional resistors serving for measuring the phototube current and the Q -factor of the circuit.

The phototube is illuminated by an incandescent light bulb (6 V, 5 W). The light bulb is powered by the *Positive ramp up wave* voltage from the *Power amplifier II*. A sensitive RMS/DC converter measures the noise voltage across the LCR circuit and produces a DC voltage for the data-acquisition system (Fig. 5). As the converter, we use the Hewlett-Packard 400E RMS voltmeter. A full-scale AC input voltage produces a 1 V DC output voltage. With the 1-mV scale, the voltmeter serves simultaneously as an amplifier with a gain of $G = 10^3$ and as a RMS/DC converter.

For the setup, the intrinsic noise at the input of the RMS/DC converter does not exceed 50 μ V. The noise voltages amount to only 20% of the 1-mV range, but this is sufficient for the measurements. The

shot noise can be observed directly with an oscilloscope. However, its connection may cause additional interference to the converter, so the oscilloscope should be disconnected when measuring the shot noise. The phototube current is measured through the voltage drop across the resistor R_1 ($10 \text{ k}\Omega$, 1%). To reduce AC voltages due to interference, the resistor is shunted by a $5\text{-}\mu\text{F}$ capacitor. The DC voltage applied to the photocell is 150 V, and the maximum current under illumination is $100 \mu\text{A}$. The *LCR* circuit and the photocell are housed in a grounded metal box. The light bulb illuminates the phototube through a hole in it.

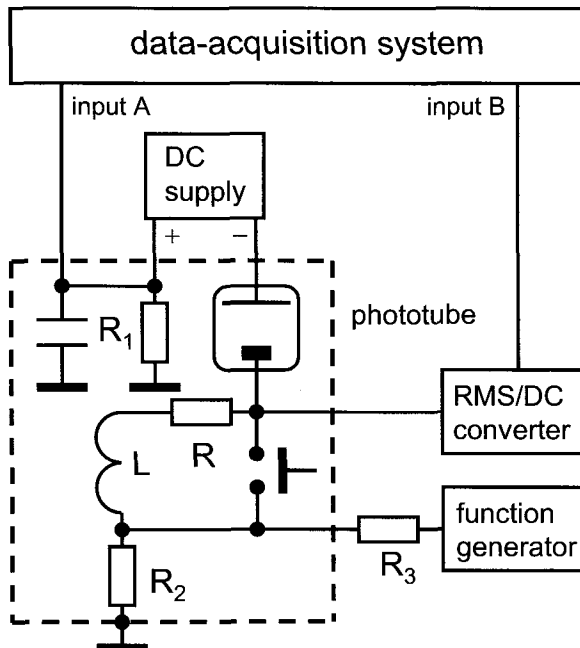


Fig. 5. Diagram of the setup. $R_1 = 10 \text{ k}\Omega$ (1%), $R_2 = 1 \Omega$, $R_3 = 1 \text{ k}\Omega$.

In the first part of the experiment, the Q -factor of the *LCR* circuit is determined for several values of the phototube current I . In this measurement, a separate DC supply feeds the light bulb illuminating the photocell. When measuring the Q -factor, the elements of the *LCR* circuit are connected in series with the source of the driving voltage. The latter is the voltage across the resistor $R_2 = 1 \Omega$ connected to the function generator in series with the resistor $R_3 = 1 \text{ k}\Omega$ positioned outside the metal box. The measurements are based on the well-known fact that at resonance the voltage on the capacitor (and the inductor) of a series *LCR* circuit becomes Q times larger than the driving voltage. An additional

complication arises because the resonance frequency also depends on the photocell current. The measurements of the voltage across the capacitor are made in the vicinity of the resonance using frequency scanning. For this purpose, an infra low frequency voltage from the *Signal generator* modifies the frequency of the function generator by using its VCF (voltage controlling frequency) input. *ScienceWorkshop* or an additional multimeter measures the phototube current through the voltage across the resistor R_1 .

The *Graph* displays the DC output voltage of the RMS/DC converter versus the voltage of the *Signal generator*, so that it is easy to determine the maximum voltage on the capacitor C . The driving voltage is set to be one order of magnitude larger than the noise. It is measured when shortening the inductor L by a switch. One thus obtains the dependence of the Q -factor on the phototube current (Fig. 6). The main change of the Q -factor occurs at currents below 20 μA . This part is of minor significance and may be excluded for the approximation of the dependence of the Q -factor on the phototube current with a polynomial. The change in the resonance frequency with the current can be neglected.

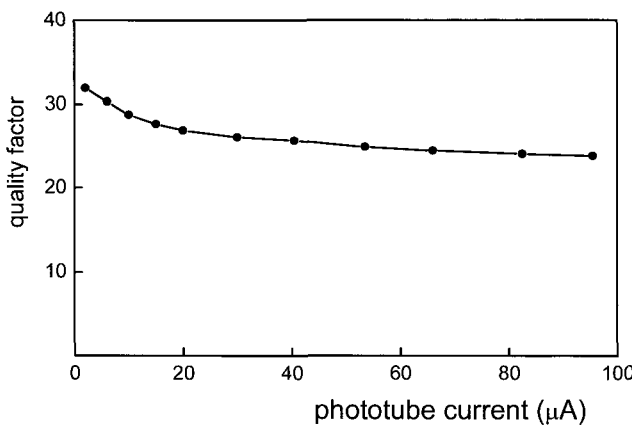


Fig. 6. Q -factor of the LCR circuit versus the phototube current I .

The capacitance of the LCR circuit includes the capacitance of the wiring, the cable connecting it to the RMS/DC converter, and the converter's input. The smaller the capacitance, the larger the shot noise voltage. Therefore, no special capacitor is included in our LCR circuit. The capacitance can be calculated from the resonance frequency ω_0 and the inductance L . The inductor has no magnetic core, so that its inductance does not depend on the current or the frequency. Any method of measuring the inductance is thus appropriate. The simplest way is to

determine the resonance frequency of a series circuit formed by the inductor and a known capacitor.

In the second part of the experiment, the period of the *Positive ramp up wave* voltage feeding the light bulb is set to be 200 s. With proper setting of the *Options*, the data acquisition starts after the first 100 s of this period, when the illumination of the phototube becomes sufficient to cause a current above 10 μA . The data acquisition ends 99 s later, 1 s before the sudden drop of the current passing through the light bulb. *DataStudio* calculates and displays the mean value of the square of the amplified noise voltage, $G^2\langle V^2 \rangle$, versus IQ . According to Eq. (11), the slope of the straight line (Fig. 7) is $K = eG^2/2\omega_0C^2$, where G is the gain of the RMS/DC converter. The dependence of Q on I is known from the polynomial previously evaluated.

All the quantities necessary for the determination of the electron charge are known from the measurements. Usually, values obtained for the electron charge differ by not more than 5% from the accepted value. For the data presented, $K = 9.42 \text{ V}^2\cdot\text{A}^{-1}$, $G = 1000$, $\omega_0 = 8.17 \times 10^5 \text{ s}^{-1}$, $L = 14.8 \text{ mH}$, $C = 101 \text{ pF}$, and $e = 1.57 \times 10^{-19} \text{ C}$. For a demonstration, one may use, with little loss of accuracy, a constant value of the Q -factor.

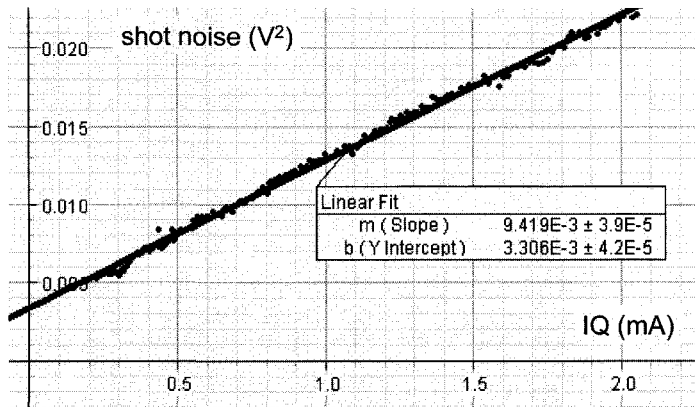
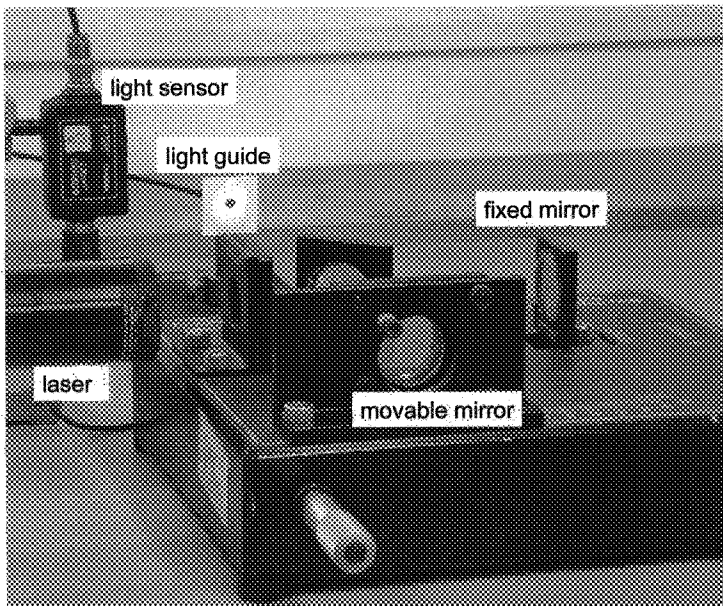


Fig. 7. Mean square of the amplified noise voltage versus IQ .

6.2. Michelson interferometer

Experiments presented employ a model of Michelson's interferometer from PASCO scientific.



Michelson's interferometer from PASCO scientific
with the *Light sensor* and a light guide added.

Additional equipment:

PASCO's interferometer, *Light sensor*, *Rotary motion sensor*, He–Ne laser, light guide.



© The Nobel Foundation
Albert Abraham Michelson
(1852–1931)

“... The foregoing will suffice not only to explain... the comprehensive and fundamental nature of Michelson’s research in one of the most difficult fields of precision physics, but also to demonstrate how fully justified is the decision of this Academy to reward it with the Nobel Prize in Physics.”

K. B. Hasselberg, member of the Royal Swedish Academy of Sciences. Presentation of Albert Abraham Michelson awarded the Nobel Prize “for his optical precision instruments and the spectroscopic and metrological investigations carried out with their aid” (1907).

Michelson’s interferometer

Michelson’s interferometer is an instrument that widely separates two beams from a single source and then brings them to one point for observing their interference. The way of obtaining the two beams is to use a semi-transparent mirror set at 45° to the axis of the incident light. It is even possible to prepare a mirror so that the two beams have the same amplitude. This achievement is due to Albert Abraham Michelson. The operation of Michelson’s interferometer is very clear (Tenquist *et al.* 1969–1970). The light beam is incident upon an accurately plane-parallel plate of homogeneous glass set at 45° to it (Fig. 1). The back surface of the plate is coated with a semi-transparent film of aluminium. After refraction in the plate, the incident beam is equally divided into two beams perpendicular to one another. The plate thus serves as a beam

splitter. One of the two beams is reflected from a fixed mirror, and the second from a movable mirror. Then the reflected beams are brought together and continue towards an observer. An additional glass plate parallel to the beam splitter is introduced to make the paths of both beams identical. If the two mirrors are accurately perpendicular to one another, a set of concentric circular interference fringes of equal inclination is seen on a screen. When one of the mirrors is slightly tilted from the perpendicular position, one can see fringes of equal thickness.

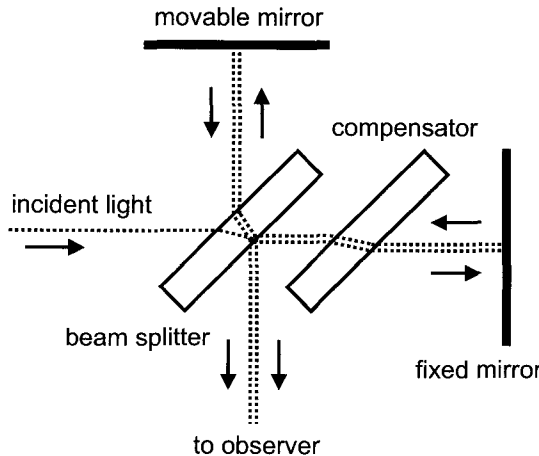


Fig. 1. Arrangement of the Michelson interferometer.

Applications of Michelson's interferometer include measurements of the light wavelength or of a geometrical length, determinations of refractive indices, or studies of the fine structure of spectral lines. In 1892–1893, Michelson and Benoît performed a comparison of the standard meter with the wavelength of light of a cadmium lamp. For a long time, the basic unit of length, the meter, was defined using a certain wavelength. Quite another definition of the meter is accepted now. It is defined as the length necessary for light to pass (in vacuum) in a definite time.

Many papers have been published on the use of Michelson's interferometer in student laboratories. Dutton *et al.* (1964) described some demonstrations using a gas laser, including a demonstration of the Doppler effect. Whiteside (1965) modified the interferometer for long-path difference and for combining beams emitted from opposite ends of a 0.1-mW He-Ne laser. The 12-m path difference served to show the long coherence length of the laser beam. Shamir and Fox (1967) used an interferometer of Mach-Zehnder type (Fig. 2) for demonstrating the

square relation between the electric vector and the intensity of the light beam, and energy conservation in interference phenomena. Yap (1971) measured the refractive index of a gas by placing an air-tight transparent cylinder in one arm of a Michelson interferometer (such an experiment is now offered by PASCO). Berkey and King (1972) used an interferometer with a photosensitive detector as a Fourier-transform spectrometer. They demonstrated interferograms of white light and of light from a He–Ne laser and a mercury lamp.

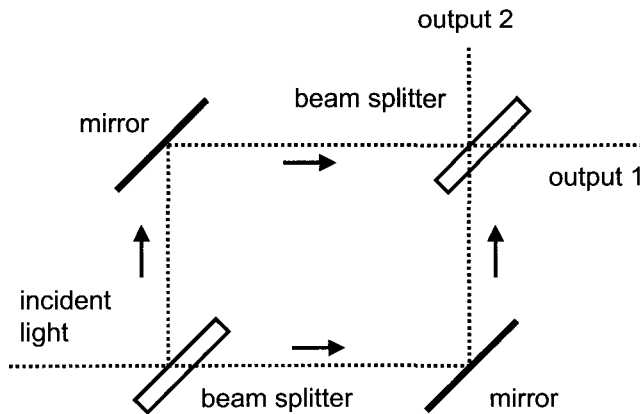


Fig. 2. Arrangement of the Mach–Zehnder interferometer.

With a Michelson interferometer, D'Iorio *et al.* (1975) determined the coherence length of the 546-nm line of a mercury lamp as a function of the voltage applied to it. The coherence length varied from about 1 to 2.5 mm. Da Costa *et al.* (1988) employed a Michelson interferometer with an optoelectronic sensor for recording small mechanical oscillations. Mellen (1990) described experiments with circularly polarized light. Rudmin *et al.* (1980) used a Michelson interferometer for producing holograms. Diamond *et al.* (1990) measured small vibrations produced by a loudspeaker. Belansky and Wanser (1993) reported on a student experiment on laser Doppler velocimetry. A spectrum analyzer was used to determine the frequency shift produced by the motion of the moving mirror. Nachman (1995) considered the Mach–Zehnder interferometer. The students set up such an interferometer from ready components. Nachman *et al.* (1997) employed an interferometer for detecting mechanical resonance of a piezoelectric element. With a photodiode and an oscilloscope, the amplitude and phase characteristics of the element are available. Kovács *et al.* (1998) used a diffraction grating when observing white-light interference fringes at the output of a

Michelson interferometer. The spectrally resolved fringes were observed with a charge-coupled device chip. Fox *et al.* (1999) described a low-cost Michelson wavemeter with picometer accuracy. By recording white-light fringes, Cormack *et al.* (2000) measured the group velocity dispersion of a crystal and of the reflectivity of a silver-coated mirror. Freschi *et al.* (2003) presented an experiment that combines opto-mechanical and electrical measurements for the characterization of a loudspeaker.

The basic interferometer from PASCO scientific (OS-9255A) can be operated in either the Michelson or Fabry-Pérot mode.

For observations of fringe patterns of equal inclination, one needs to adjust the positions of the two mirrors and to make them accurately perpendicular to one another. In this case, one sees concentric fringes of equal inclination on the screen. Then by slightly tilting the movable mirror equipped with adjusting screws one observes fringes of equal thickness (Fig. 3).

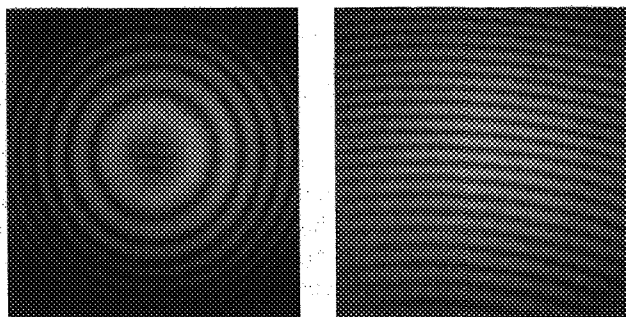


Fig. 3. Fringe patterns of equal inclination and of equal thickness.

Since the interfering light beams are widely separated, it is easy to add polarizers in the paths of the light. Then one observes the change in the interference fringes when changing the orientation of the polarizers.

Determination of the light wavelength

This experiment demands slowly moving the movable mirror using a special micrometer head and simultaneously count the disappearance of circular dark fringes in the center of the pattern. To make the measurements easier, we use the *Light sensor* and a light guide, whose entrance is positioned in the center of the interference fringes. *DataStudio* displays electrical pulses from the sensor on the screen (Fig. 4), and then it becomes easier to count them. The measurements are

carried out with a 25- μm displacement of the moving mirror, so that the change in the optical path is 50 μm . The measurements are repeated several times. The next step in this experiment should be an automated count of the interference fringes.

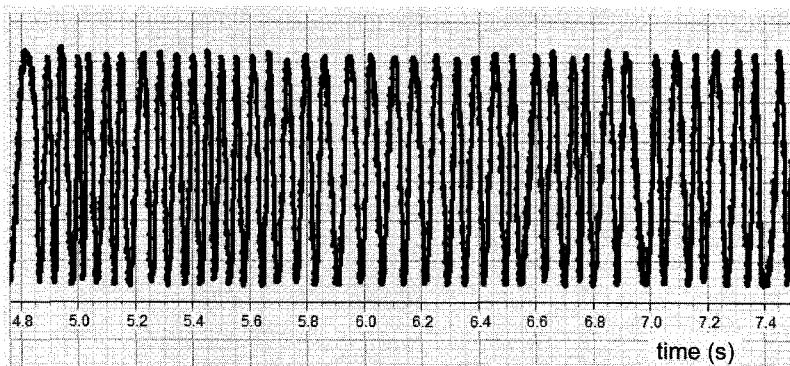


Fig. 4. Example of records by *DataStudio* when measuring the wavelength.

Refraction index of air

The measurements involve slow evacuation of the gas from a special gas cell also provided by PASCO. The dependence of the refraction index of air on its temperature can be seen from distortions in fringes of equal thickness when a small heater is placed under the light path in one arm of the interferometer.

Refraction index of glass

The aim of this experiment should not be considered as a determination of the refraction index of glass because other methods known for this purpose are much more accurate. The experiment is an additional demonstration of the interference of light and of the Michelson interferometer. The measurements are performed by introducing a plane-parallel glass plate in one arm of the interferometer. First the plate is positioned to be perpendicular to the light beam. Then one slightly rotates the plate and observes the disappearance of circular dark fringes in the center of the pattern. To make the measurements easier, the *Rotary motion sensor* measures the angle position of the plate α . Simultaneously, the *Light sensor* measures the intensity of light in the center of the interference pattern. The angular resolution of the *Rotary*

motion sensor (0.25°) is sufficient only when the incident angles are close to zero. For measurements at large incident angles, a gear reducer is introduced (Fig. 5). *DataStudio* displays the signal from the sensor versus $1/\cos\beta - 1$, where β is the refraction angle. The refraction index was assumed to be 1.5. Now the peaks of light intensity become equidistant (Fig. 6).

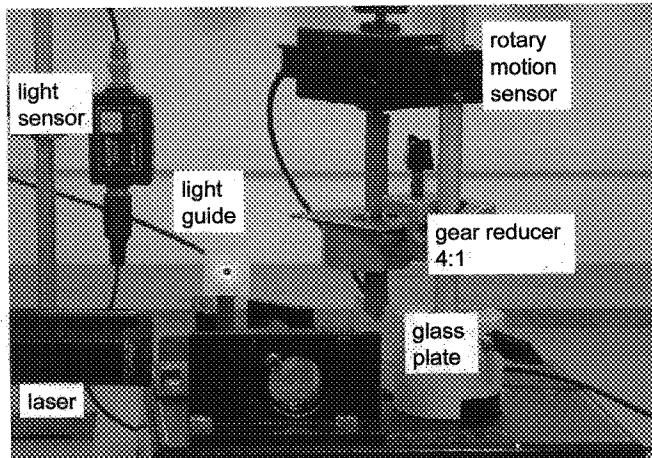


Fig. 5. Arrangement for the determination of the refractive index of glass.

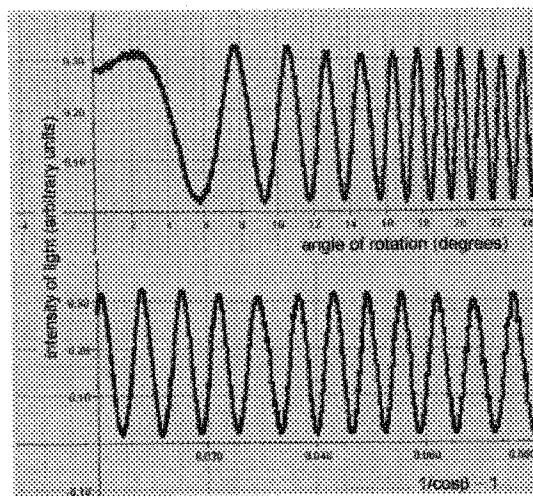


Fig. 6. With a scale $1/\cos\beta - 1$, the peaks of light intensity become equidistant.

Doppler effect

To demonstrate the Doppler effect, we use the PASCO's *Mechanical wave driver* (SF-9324), to which a plane mirror is attached. The driver is fed by the *Sine waveform* voltage. The interference fringes are viewed by a photodiode (Fig. 7). Its output voltage is displayed by the *Scope* tool (Fig. 8) and fed to an audio amplifier and then to a loudspeaker.

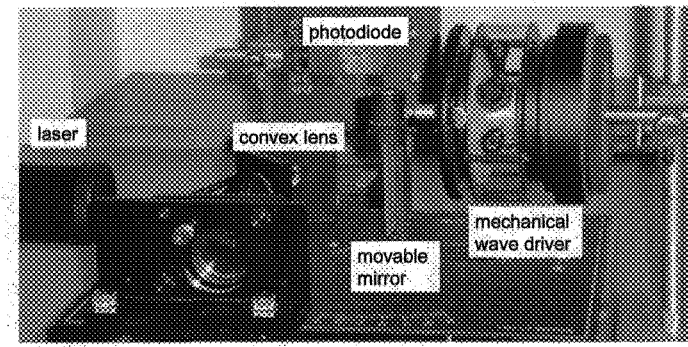


Fig. 7. Arrangement for demonstrating the Doppler effect.
Note the position of the convex lens.

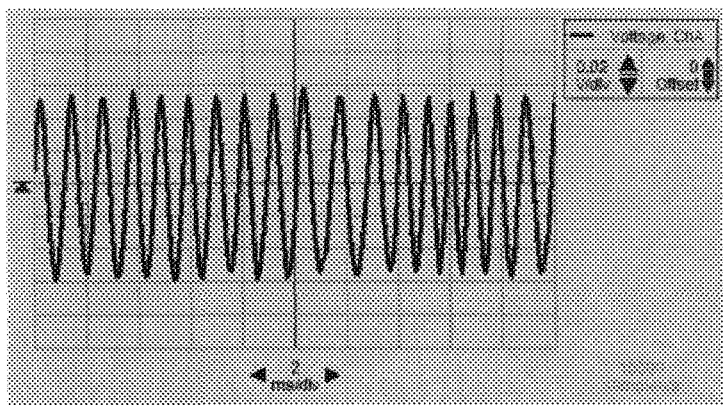
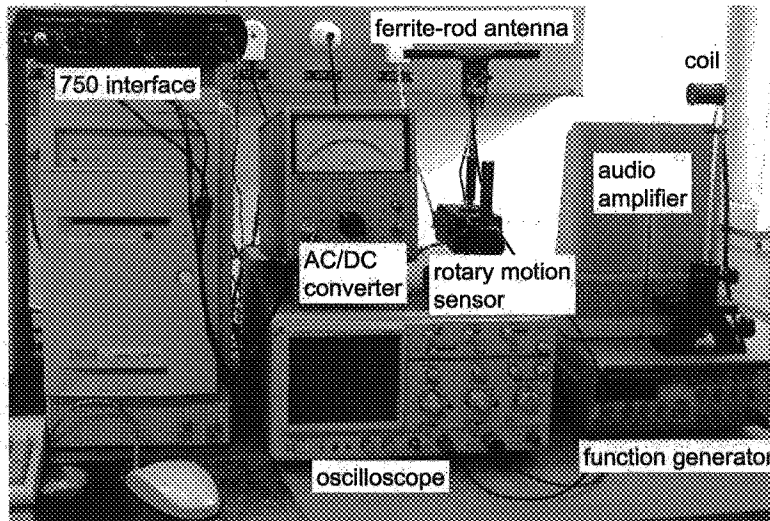


Fig. 8. The signal from the photodiode due to the Doppler effect.

6.3. Principles of radio

A simple setup illustrates the amplitude modulation and demodulation, the selectivity of a radio receiver, and the features of a directional antenna (Kraftmakher 2002c).



The experimental setup.

Additional equipment:

Rotary motion sensor, Voltage sensor, oscilloscope, ferrite-rod antenna, varicap, function generator with digital frequency indication, coil, AC/DC converter, audio amplifier with loudspeaker, semiconductor diode, three resistors, two capacitors.



© The Nobel Foundation
Guglielmo Marconi
(1874–1937)



© The Nobel Foundation
Carl Ferdinand Braun
(1850–1918)

“...Research workers and engineers toil unceasingly on the development of wireless telegraphy. Where this development can lead, we do not know. However, with the results already achieved, telegraphy over wires has been extended by this invention in the most fortunate way. Independent of fixed conductor routes and independent of space, we can produce connections between far-distant places, over far-reaching waters and deserts. This is the magnificent practical invention which has flowered upon one of the most brilliant scientific discovery of our time!”

H. Hildebrand, President of the Royal Swedish Academy of Sciences. Presentation of Guglielmo Marconi and Carl Ferdinand Braun awarded “in recognition of their contributions to the development of wireless telegraphy” (1909).

In 1895, Marconi succeeded in sending wireless signals over a distance of one and a half miles, thus becoming the inventor of the first practical system of wireless telegraphy. In 1899, he established wireless communication between France and England. In 1901, Marconi used his system for transmitting signals across the Atlantic.

In 1897, Braun invented a cathode-ray tube. In 1898, he attempted to transmit Morse signals through water by means of high-frequency currents. Braun was one of the first to send electromagnetic waves in definite directions. Braun's papers were published in 1901 in a brochure “*Drahtlose Telegraphie durch Wasser und Luft*.”

Modulation and demodulation

Only few technical achievements play in our life a role comparable to that of radio and television. Regrettably, few physics textbooks pay attention to this subject. The textbook by Hecht (1994) that tells somewhat about radio communications and describes a simple radio receiver is rather an exception. Many sources provide a description of the principles of radio. The *McGraw-Hill Encyclopedia* (Parker 1997) serves here as a handbook.

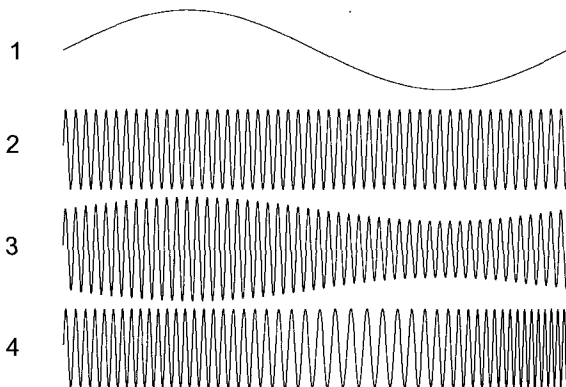


Fig. 1. Waveforms of signals for radio communications: 1 – low-frequency signal, 2 – high-frequency carrier, 3 – amplitude modulation, 4 – frequency modulation.

For radio communications, the information to be transmitted must cause amplitude or frequency modulation of a high-frequency carrier (Fig. 1). Amplitude modulation (AM) is the oldest form of modulation. The amplitude of the high-frequency wave is varied in response to a low-frequency signal. This technique is used in AM broadcasting, television picture transmission, radiotelephony and radiotelegraphy, and navigational aids. Each radio transmitter operates within a specific radio-frequency channel. The minimum usable channel widths depend upon the amount of information a channel must transmit. With amplitude modulation, when a sine wave of frequency Ω modulates a sine wave of frequency ω , the resulting oscillation is

$$(1 + m\sin\Omega t) \sin\omega t = \sin\omega t + (m/2)\cos[(\omega - \Omega)t] - (m/2)\cos[(\omega + \Omega)t], \quad (1)$$

where $m < 1$ is the so-called modulation index.

This equation shows that the amplitude-modulation process generates new frequencies, called side frequencies or side bands (Fig. 2). AM signals have identical upper and lower sidebands symmetrically located on each side of the carrier. The necessary channel width depends on the upper frequency of the signal used for the modulation. In AM broadcasting, the channel width is 10 kHz. In television, it is 6 MHz because of a large amount of essential video information. Frequency modulation is used in FM broadcasting, television sound transmission, and microwave relaying. In FM broadcasting, the channel width is 200 kHz. The insufficient bandwidth in AM broadcasting limits the quality of musical transmissions. The FM broadcasting improves the situation but needs to use very high carrier frequencies. The single-sideband technique reduces the necessary bandwidth.

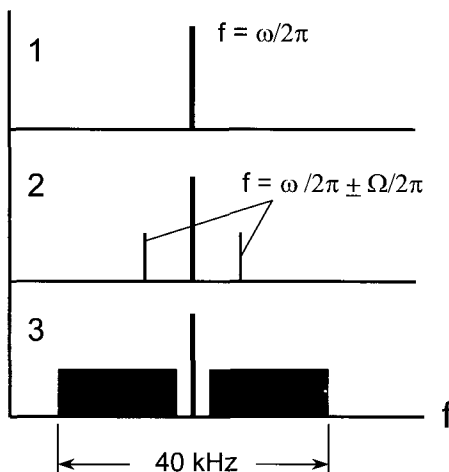


Fig. 2. Spectra of radio signals. 1 – unmodulated carrier, 2 – AM by single frequency, 3 – AM by a 20 Hz–20 kHz audio band.

At a broadcasting station, a low-frequency signal modulates a high-frequency carrier, and the corresponding modulated current is sent to an antenna. The antenna creates high-frequency electromagnetic waves, which induce a voltage in an antenna of a radio receiver. This signal is selected by tuning the antenna circuit, and then amplified and demodulated. The low frequency signal obtained by the demodulation reproduces the signal used for the modulation at the broadcasting station (Fig. 3).

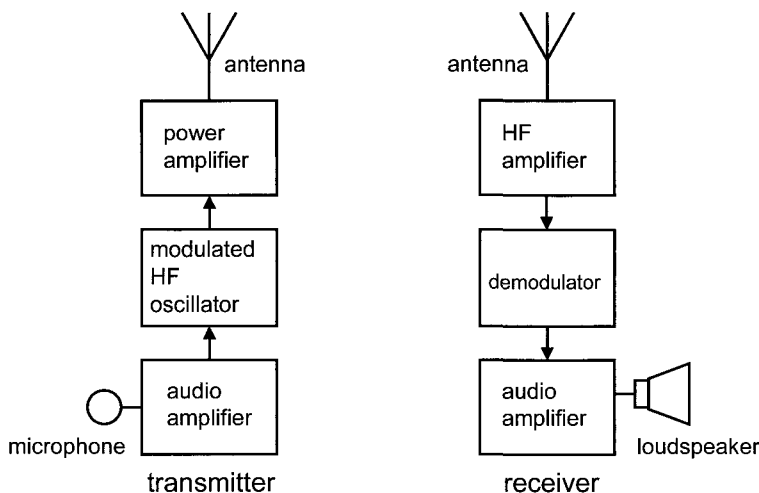


Fig. 3. Scheme of radio broadcasting.

The receiver must select and sort the low-frequency signals from the high-frequency carrier. The simplest AM-broadcasting receiver consists of an antenna, a tuneable band-pass filter, a high-frequency amplifier, a demodulator, a low-pass filter, and an audio amplifier with a loudspeaker (Fig. 4). Such a receiver is called the tuned-radio-frequency receiver. The simplest demodulator employs a semiconductor diode. More complex methods of demodulation are now in use. They consist of creating a sine wave voltage of the same frequency and phase that the broadcast carrier has. This can be done, for instance, by means of a limiting amplifier. The amplifier provides a voltage of the same sign as the input voltage but of constant magnitude. To obtain the audio signal, it is enough to multiply the broadcast signal by the created voltage and to smooth the product. Tuned-radio-frequency receivers are now out of use because they do not provide the necessary selectivity. Modern radio receivers, so-called superheterodynes, employ the frequency-conversion technique. In such a receiver, the high-frequency signal passes to a frequency converter. The converter includes a local oscillator and a mixer, which translates the high-frequency signal to a signal of an intermediate frequency (IF). This frequency does not depend on the frequency of the original signal, so that there is no need for tuning the IF amplifier. The amplitude modulation of the intermediate-frequency voltage reproduces the original modulation. A high-performance fixed-frequency filter follows the frequency converter and ensures the necessary selectivity of the receiver.

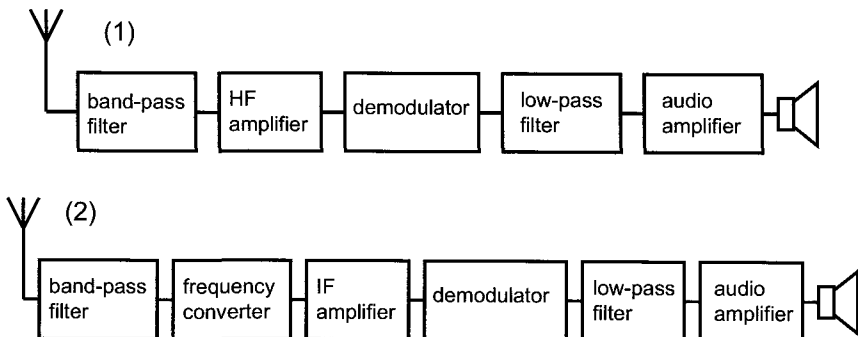


Fig. 4. Structures of a tuned-radio-frequency receiver and of a superheterodyne receiver.

Experimental setup

The experiment illustrates the main principles of radio: modulation and demodulation, the selectivity of a radio receiver, and the features of a directional antenna. A simple radio setup for AM signals serves for this purpose (Fig. 5). It includes a ferrite-rod antenna with a variable capacitor, a high-frequency (HF) amplifier, a semiconductor diode (demodulator), and an audio amplifier with a loudspeaker. The ferrite-rod antenna is a coil wrapped about a ferrite rod. The setup thus represents the simplest tuned-radio-frequency receiver.

A two-channel oscilloscope (*e.g.*, Good Will model GOS-622G or Kenwood model CS-4025) amplifies the antenna's signals and displays modulated high-frequency signals and audio signals. The oscilloscope has an output terminal from one of the channels, with the usable gain up to 100. An integrating RC circuit follows the demodulator. It suppresses high-frequency voltages but retains low-frequency oscillations for the audio amplifier. Two sensors are used, the *Rotary motion sensor* and the *Voltage sensor*. A varicap (*e.g.*, BB112 from Philips Electronics) acts as the variable capacitor governed by an external DC voltage. The varicap (also known as varactor) uses a $p-n$ junction and has a structure such that the capacitance of the diode varies with the applied voltage. The *Signal generator* provides this voltage. An AC/DC converter supplies a DC voltage for the *Voltage sensor*. This voltage is proportional to the high-frequency oscillations in the antenna circuit. A DC voltage nearly proportional to the antenna's signal could be taken from the demodulator. However, because of the nonlinearity of the latter, the use of an AC/DC converter is preferable.

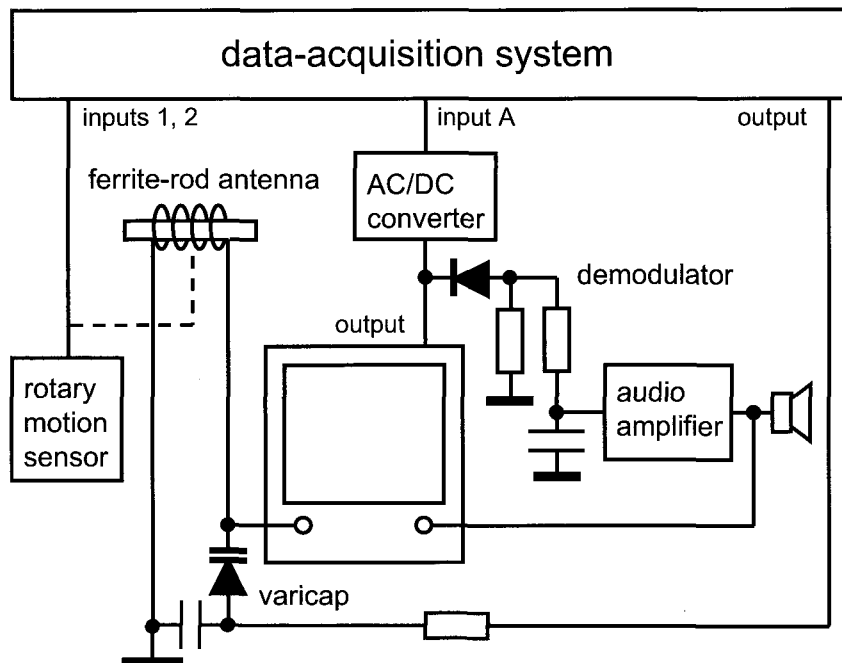


Fig. 5. Diagram of the setup for the measurements. The oscilloscope serves also for amplifying high-frequency signals.

The experiment consists of several parts including the observation of AM high-frequency signals and audio-frequency oscillations from a broadcasting station by means of the two-channel oscilloscope. Simultaneously, the students are listening to the broadcast. The tuning of the receiver is done by changing the voltage applied to the varicap. The *Signal generator* provides this DC voltage.

Calibration of the receiver

A coil inductively coupled to the ferrite-rod antenna is connected to the output of a function generator with digital frequency indication (*e.g.*, Good Will model GFG 8019G). This approach uses Faraday's induction law. The students calibrate the antenna resonant circuit by stepwise changing the voltage applied to the varicap and tuning the function generator. From the data, a graph and a polynomial fit are available (Fig. 6).

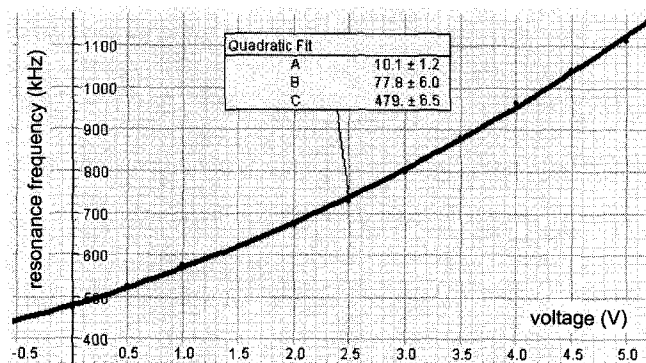


Fig. 6. Resonance frequency versus voltage applied to the varicap.

Selectivity of antenna circuit

The resonance curve of the antenna circuit is measured by means of a weak frequency modulation of the function generator. The *Signal generator* provides a 0.01 Hz *Sine wave* voltage for the modulation, and the *Voltage sensor* measures the output voltage from the AC/DC converter. The voltage used for the frequency modulation is also stored. To translate this voltage into frequency, a preliminary calibration is necessary. The resonance curve is a graph of the AC/DC converter's output voltage versus frequency (Fig. 7). For the frequency of 1 MHz, the bandwidth of the antenna circuit well matches the channel width used in AM broadcasting. For a carrier frequency of 10 MHz, the resonance curve of a circuit of the same quality is ten times broader and does not provide the necessary selectivity. Superheterodyne receivers must be used at such frequencies corresponding to short waves.

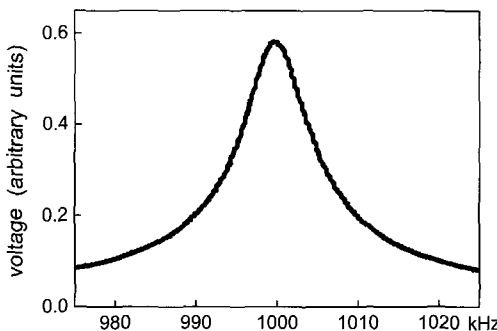


Fig. 7. Resonance curve of the antenna circuit tuned to 1 MHz.

Panorama of accessible broadcasting stations

To determine frequencies and relative amplitudes of the electromagnetic fields of accessible broadcasting stations, the *Positive ramp up wave* voltage from the *Signal generator* (5 V) feeds the varicap. The frequency of this voltage is 0.002 Hz. The voltage is translated into frequency using the polynomial fit obtained by the calibration. Two perpendicular orientations of the ferrite-rod antenna are necessary for determining correct amplitudes of the electromagnetic fields (Fig. 8).

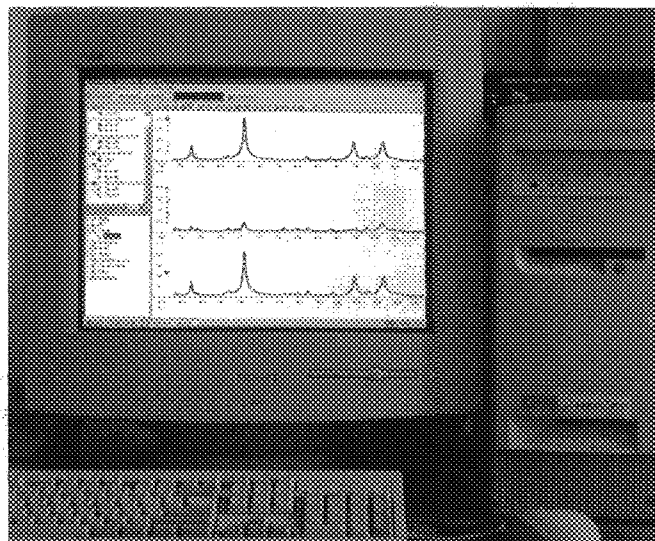


Fig. 8. Runs with two perpendicular orientations of the antenna (*A* and *B*) provide correct amplitudes of the electromagnetic fields ($C^2 = A^2 + B^2$).

Directivity diagram of antenna

For this measurement, one should find a sufficiently strong broadcasting station. The directivity diagram of the ferrite-rod antenna is measured with the *Rotary motion sensor*. The angle range from 0 to 360° limits the measurements by properly setting the *Automatic stop*. The directivity diagram (Fig. 9) is obtainable with the *Origin* software. The diagram is in reasonable agreement with the theory: the signal should be proportional to the sine of the angle between the axis of the antenna and the direction to the transmitting station. The diagram confirms that electromagnetic waves are transverse. To convert the data to polar

coordinates with *DataStudio*, one uses the *Calculate* tool to create functions $y = r\sin\phi$ and $x = r\cos\phi$ and then plots a graph $y(x)$.

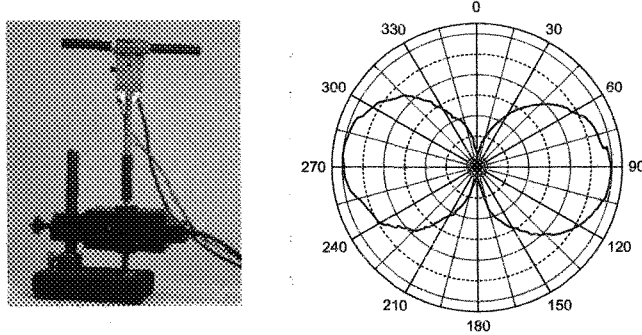


Fig. 9. The ferrite-rod antenna mounted on the axle of the *Rotary motion sensor* and its directivity diagram.

This experiment is possible without a data-acquisition system. In this case, a DC voltage to the varicap is obtained from an adjustable DC source. This voltage is used for the calibration of the receiver and then for determining the panorama of accessible broadcasting stations. To correctly measure the amplitudes of the electromagnetic fields produced by different stations, the stations are found by changing the DC voltage applied to the varicap. The orientation of the antenna should be adjusted every time to achieve a maximum signal. For the measurement of the directivity pattern of the antenna, one mounts the antenna on the axle of a many-turn potentiometer (Fig. 10). The DC voltage applied to the potentiometer is adjusted to obtain a 360-mV readout per turn. A digital multimeter measures the output voltage of the potentiometer.

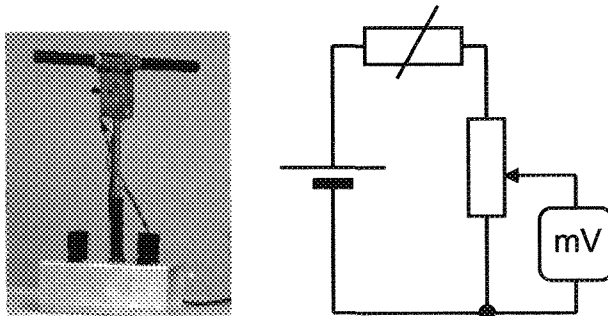
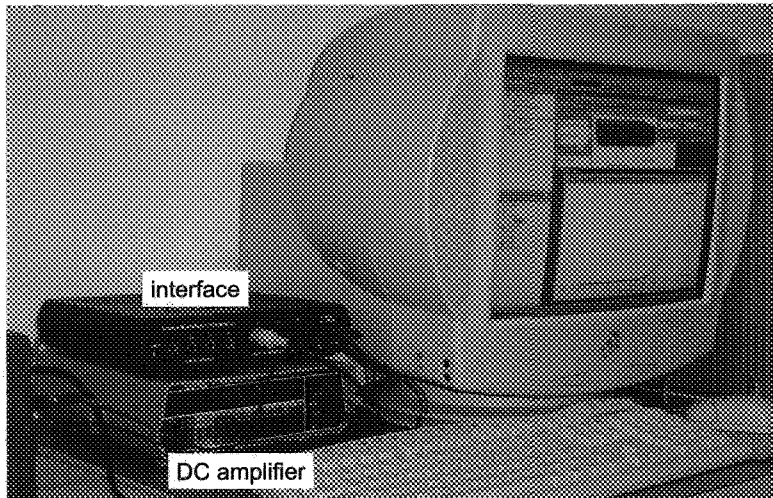


Fig. 10. The ferrite-rod antenna mounted on the axle of a potentiometer.

6.4. Photoelectric effect

The h/e ratio is determined from the photoelectric effect. The use of a data-acquisition system allows one to introduce a correction for a leakage current in the phototube and determine the stopping potential more reliably. The work function is determined from the photoemission threshold (Kraftmakher 2006d).

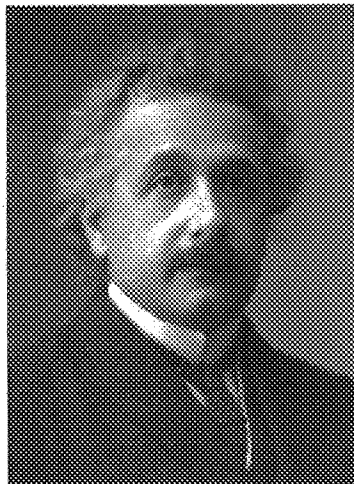


Additional equipment:

Voltage sensor, vacuum phototube, light bulb, lens, monochromator, DC amplifier, DC supply.



© The Nobel Foundation
Robert Andrews Millikan
 (1868–1953)



© The Nobel Foundation
Albert Einstein
 (1879–1955)

“...Millikan’s aim was to prove that electricity really has the atomic structure... It was necessary to measure the charge of a single ion with such a degree of accuracy as would enable him to ascertain that this charge is always the same, and it was necessary to furnish the same proofs in the case of free electrons. By a brilliant method of investigation and by extraordinarily exact experimental technique Millikan reached his goal.”

A. Gullstrand, Chairman of the Nobel Committee for Physics. Presentation of Robert Andrews Millikan awarded the Nobel Prize “for his work on the elementary charge of electricity and on the photoelectric effect” (1923).

“...There is probably no physicist living today whose name has become so widely known as that of Albert Einstein... Einstein’s law has become the basis of quantitative photochemistry in the same way as Faraday’s law is the basis of electrochemistry.”

S. Arrhenius, Chairman of the Nobel Committee for Physics. Presentation of Albert Einstein awarded the Nobel Prize “for his services to Theoretical Physics, and especially for his discovery of the law of the photoelectric effect” (1921).

Planck's constant, Einstein's equation, and Millikan's experiment

Measurement of the h/e ratio (where e is the electron charge) from the photoelectric effect is an experiment introducing students to quantum physics. During decades, many papers were published on this experiment, and only a fraction of them is mentioned here. Hanson and Clotfelter (1966) presented an evaluation of equipment commercially available for determining the h/e ratio in student laboratories. The authors stressed that certain practical problems encountered in this experiment make good results difficult to obtain. In particular, a serious problem is caused by the emission of electrons from the anode. The Leybold's apparatus includes a vacuum phototube with an anode in the form of a platinum wire loop that can be heated shortly before taking data. The purpose of the heating is to vaporize any material that has condensed on the anode from the photocathode. It turned out that the results obtained strongly depend on this procedure. Hall and Tuttle (1971) used an AC amplifier for measuring the photocurrent caused by an AC-powered mercury arc. Hall (1971) developed an efficient amplifier for AC photoelectric measurements. Carver and Crawford (1975) described a demonstration of the photoelectric threshold. Powell (1978) justified a procedure often used to determine the stopping potential from a plot of photocurrent root squared versus applied bias voltage. Steinberg *et al.* (1996) developed a computer-based tutorial on the photoelectric effect.

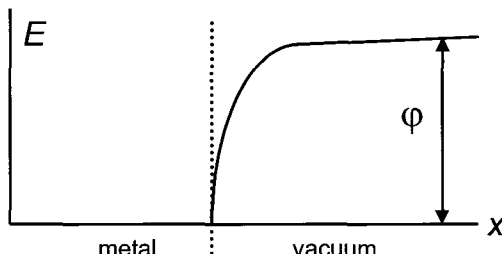


Fig. 1. Simplified diagram of potential barrier at the boundary between metal and vacuum and definition of the work function.

Under normal conditions, free electrons that move inside metals cannot leave them and escape outwards. This means that a potential barrier exists at the surface of the metal that prevents electrons from leaving it. The energy necessary for an electron to leave the metal at the absolute zero temperature is called the work function φ (Fig. 1). Several

sources are known to deliver to the electron the necessary energy: the thermal motion (thermionic emission), quanta of light (photoelectric effect), and bombardment by electrons or other particles (secondary electron emission).

The photoelectric effect manifests peculiarities that cannot be explained by the wave theory of light. The energy of electrons leaving the cathode is independent of the intensity of incident light, but it depends on its wavelength. However, it is easy to explain the phenomenon accepting the quantum theory. Einstein has shown in 1905 that the energy conservation law fairly explains the effect. He supposed that Planck's formula $E = hf$, where h is Planck's constant and f is the frequency of light, is valid not only for atomic energy levels. Einstein's revolutionary idea was that the light is formed by particles each having this energy, and these particles are elemental portions of light. At that time, Planck did not accept this concept, but soon he became one of the adepts of the new theory. When light falls onto a metal, a free electron acquires the full energy of a photon hf . This energy is utilized to overcome the potential barrier φ , and the rest is partly consumed in interactions inside the metal. The following equation is therefore valid for electrons leaving the cathode of a vacuum phototube:

$$hf = \varphi + mv_m^2/2, \quad (1)$$

where m is the electron mass, and v_m is the maximum velocity of electrons leaving the cathode. This extremely simple and now evident relation is famous Einstein's equation. It was confirmed by Millikan's brilliant experiments.

For the determination of the maximum energy of electrons leaving the cathode (emitter) of a vacuum phototube, a negative potential that slows down the electrons is applied to the anode (collector). For the stopping potential U ,

$$eU = mv_m^2/2, \quad \text{and} \quad (2)$$

$$hf/e = \varphi/e + U. \quad (3)$$

The energy of the electrons is in the range from zero to a maximum because their energy is reduced during the escape from the emitter. In Eq. (3), the contact potential between the electrodes of the phototube was not taken into account. It was shown that the work function of the emitter entering Eq. (3) should be replaced by that of the collector (Rudnick and Tannhauser 1976). It seems to be simple to make use of Eq. (3) to determine the h/e ratio. For this purpose, one needs to determine the cut-off energies for several frequencies of incident light.

However, several complicating effects may cause the cut-off energies to be difficult to observe. Keesing (1981) listed these effects as follows:

- Point to point variation of the work function of the emitter.
- Energy dependent electron reflection at the collector.
- Geometrical effects, which cause an electron to have sufficient energy but insufficient momentum to reach the collector.
- Reverse photoelectric and leakage currents.
- Thermal effects.

Two distinct methods are known to determine the cut-off energy. The first method employs an open circuit phototube and allows the collector to charge negatively in response to the photocurrent from the emitter until no more electrons can reach it. This self-induced bias is measured as a function of the frequency of incident light. However, it was shown (Keesing 1981) that increasing the light intensity causes the cut-off energy to increase. Nevertheless, this method was used in some student experiments (Boys *et al.* 1978; Bobst and Karlow 1985; Barnett and Stokes 1988), and in the PASCO's h/e apparatus.

The second method repeats Millikan's observations of $I-U$ characteristics of a vacuum phototube. Among the complicating effects listed above, the thermal effects are of fundamental nature. Einstein's equation is strictly correct when the emitter is at the absolute zero of temperature. At any finite temperature, the thermal motion of electrons contributes to their initial velocities when leaving the emitter. Therefore, the equation becomes inapplicable (Keesing 1981). Knudsen (1983) has shown that the problem can be solved by applying Fowler's theory taking into account the emitter's temperature, and using a plane-parallel geometry of the electrodes. With these improvements, the results obtained were within 1% of the true h/e ratio. The stopping potential is measured for different frequencies of the incident light. A mercury lamp providing light of well-known spectral lines or a monochromator is needed for the measurements. The experiment was included in many university courses (Portis 1964; Portis and Young 1971; Goldin 1983; Soloukhin 1983; Meiners *et al.* 1987).

Determination of the ratio h/e

Results obtainable by using simple commercial apparatus may differ significantly from the correct h/e value. One of the reasons for this disagreement is the reverse current of electrons emitted by the collector, also due to the photoelectric effect. For these electrons, the potential applied to the phototube is an accelerating voltage. To suppress this

phenomenon, the collector should be screened from the incident light. The second drawback leading to errors in the data obtained is the insufficient isolation of the photocell. The isolation resistance, of the order of $10^{10} \Omega$, causes a reverse leakage current, which is proportional to the applied voltage. The leakage current results in errors in the determination of the stopping potential. To reduce the influence of the insufficient isolation, one can employ more intense light sources. Another possibility is to determine the leakage current as a function of the applied voltage and to introduce the necessary corrections. In any case, employment of a data-acquisition system has an important advantage because the $I-U$ characteristics are obtainable in a short time and are observable on the screen. This makes the determinations of the stopping potentials easier. In our case, the vacuum phototube is illuminated by means of a halogen light bulb and a grating monochromator (Fig. 2).

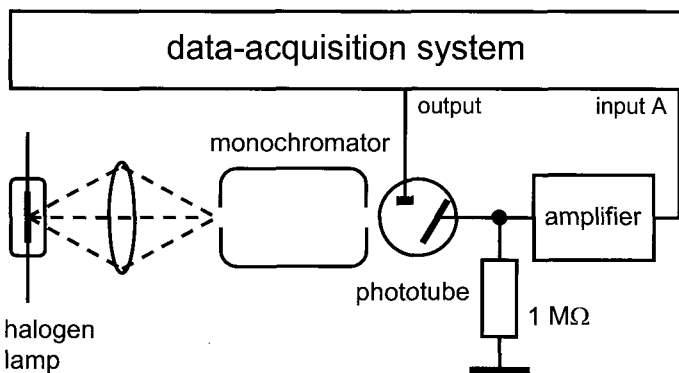


Fig. 2. Diagram of the setup for the measurements.

The load resistor of the phototube is $1 \text{ M}\Omega$. The voltage across it is amplified by the Keithley 177 model multimeter and then fed to the input of the data-acquisition system. With the 20-mV scale, the multimeter provides a 100-fold amplification. A 0.001-Hz *Sine wave* voltage from the *Signal generator* is applied to the phototube. After starting the measurements, the generator starts to reproduce the negative part of this waveform, and one run lasts 250 s. The measurements with wavelengths from 400 to 650 nm provide the $I-U$ characteristics of the phototube.

DataStudio allows the part of the characteristic close to the stopping potential to be enlarged. The *Smooth* option is useful to reduce the scatter of the experimental points. Without the illumination, the characteristic represents the leakage current (dark current) linearly

dependent on the applied voltage. Using *Fit/Linear fit*, one determines this dependence and introduces the necessary correction. Now the characteristic contains only two contributions, the photoelectric current from the emitter, and that from the collector. The latter is sufficiently small and reaches saturation at low voltages (Fig. 3). The determination of the stopping potential thus becomes easier (Fig. 4). Also important, the students clearly see all three contributions to the current flowing through the phototube. With the above procedure, the h/e ratio obtained becomes within $\pm 5\%$ of the correct value (Fig. 5).

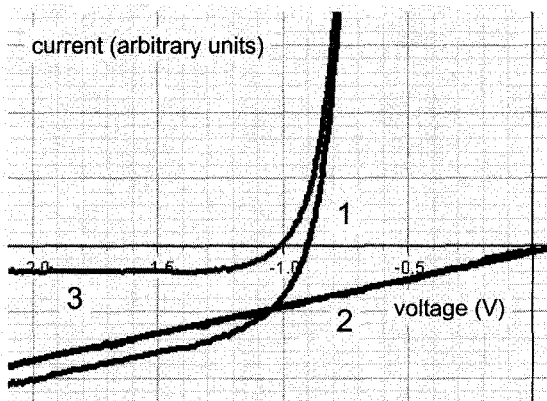


Fig. 3. Part of I - U characteristic for $\lambda = 500$ nm: 1 – original data (smoothed), 2 –contribution of the leakage current, and 3 – data corrected for the leakage.

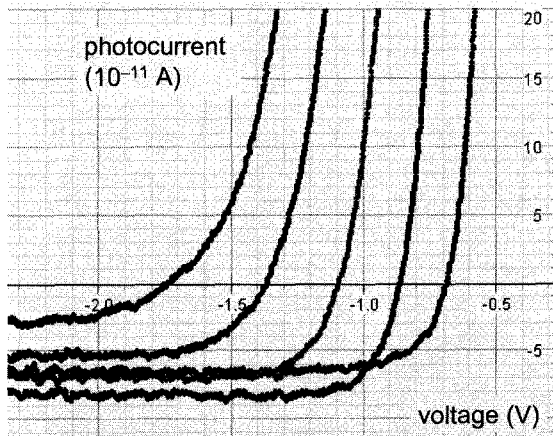


Fig. 4. Corrected I - U characteristics for various wavelengths.

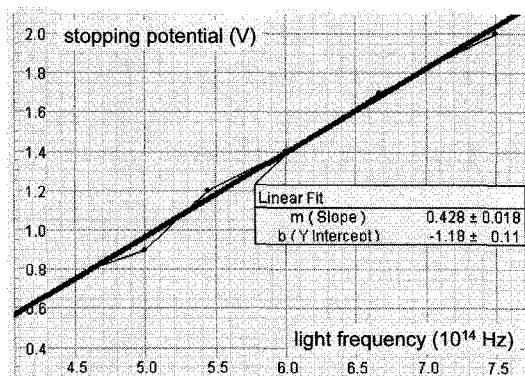


Fig. 5. Stopping potential versus the frequency of light.
From the data, $h/e = 4.28 \times 10^{-15} \text{ J.s.C}^{-1}$.

The work function

The simplest method to determine the work function is the measurement of the photoemission threshold λ_0 , the longest wavelength of light, for which the photoelectric effect is still possible (Fig. 6). The energy of quanta related to the photoemission threshold equals the work function:

$$\varphi = hf_0 = hc/\lambda_0. \quad (4)$$

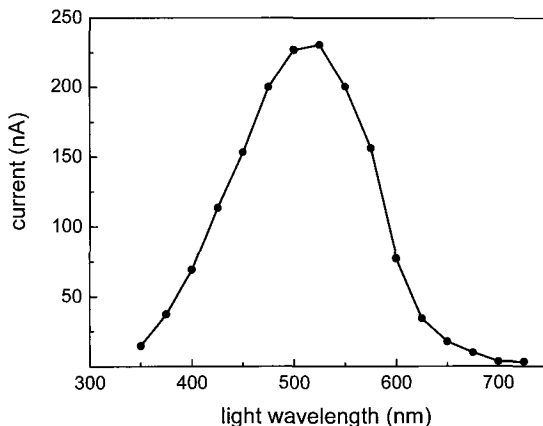
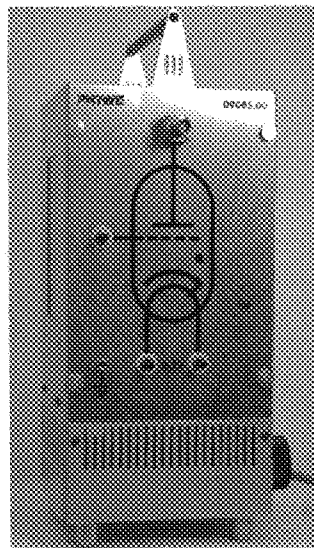


Fig. 6. The photoelectric current versus light wavelength. The photoemission threshold is about $0.7 \mu\text{m}$, so that the work function equals 1.8 eV.

6.5. Franck–Hertz experiment

Two variants of the Franck–Hertz experiment are presented. The first version is based on the apparatus from PHYWE. The second one employs a thyratron, *i.e.*, a gas-filled triode with a cathode heated by an electric current (Kraftmakher 1959a).



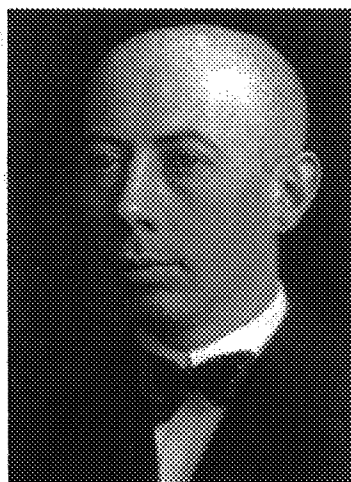
Franck–Hertz apparatus from PHYWE.

Additional equipment:

Three *Voltage sensors*, Franck–Hertz apparatus from PHYWE, DC supply, DC amplifier, thyratron.



© The Nobel Foundation
James Franck 1882–1964)



© The Nobel Foundation
Gustav Hertz (1887–1975)

“...Professor Franck. Professor Hertz. Through clear thinking and painstaking experimental work in a field which is continuously being flooded by different hypotheses, you have provided a firm footing for future research.”

C. W. Oseen, member of the Nobel Committee for Physics.
Presentation of James Franck and Gustav Hertz awarded “for their discovery of the laws governing the impact of an electron upon an atom” (1925).

In 1914, James Franck and Gustav Hertz reported on an experimental work concerning collisions between electrons and mercury atoms. A hot cathode emits electrons, which are then accelerated by a potential applied to the grid (Fig. 1). The electrons undergo collisions with mercury atoms in the space between the cathode and the grid. After the grid, the electrons arrive at a metallic plate, and the current is measured by a galvanometer. The potential of the plate is kept somewhat lower than that of the grid. Therefore, if the electrons lose their energies in the collisions, their kinetic energy may become smaller than necessary to overcome the potential barrier between the grid and the plate.

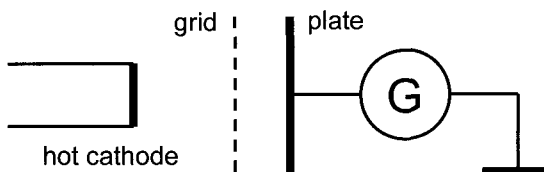


Fig. 1. Diagram of the Franck–Hertz experiment for studying collisions between electrons and mercury atoms.

When measuring the plate current versus the accelerating voltage, periodic maxima and minima are observed. If the electron kinetic energy is less than 4.9 eV, the collisions are elastic, *i.e.*, the electron can change direction but not velocity. When the energy reaches 4.9 eV, many collisions become completely inelastic, the electron gives up its entire kinetic energy to the atom. A bit above 4.9 eV many electrons still give 4.9 eV to the atom, then continue with an energy that is lower by that amount. According to Bohr's theory, this energy corresponds to the first discrete excited state. The I - U characteristic shows a minimum in the vicinity of the accelerating voltage equal to the energy level of the mercury atom. The electrons can undergo such collisions several times, so that several minima are observable when the accelerating voltage is changed over a wide range. The excited atom drops back to its original state following the emission of a photon of energy hf determined by the relation

$$hf = E_2 - E_1, \quad (1)$$

where E_2 and E_1 are the energy levels of the mercury atom.

The Franck–Hertz experiment is included in many laboratory courses (*e.g.*, Portris 1972; Goldin 1983; Melissinos and Napolitano 2003). Adelberger and Kinsey (1972), Caley (1972), and Huebner and Humphries (1974) described an experiment employing an oscilloscope. Carpenter (1975) used an X - Y recorder for displaying the electron current versus the accelerating voltage. Huebner (1976) has observed that light-emitting zones appear inside the Franck–Hertz tube. With a photomultiplier, Buhr *et al.* (1983) observed UV emission in the Franck–Hertz experiment. McMahon (1983) considered elastic electron-atom collisions. Martin and Quinn (1984) used a two-grid Franck–Hertz tube to determine electron energy-loss spectra. With a two-grid tube, Liu (1987) observed higher excitation levels of the mercury atom. Nornes and Tu (1989) developed a computer-assisted experiment. Fedak *et al.* (2003) employed the *LabVIEW* software for the automation of the experiment.

Experiment and results

Using the PHYWE apparatus and a data-acquisition system, it is easy to reproduce the Franck–Hertz experiment (Fig. 2).

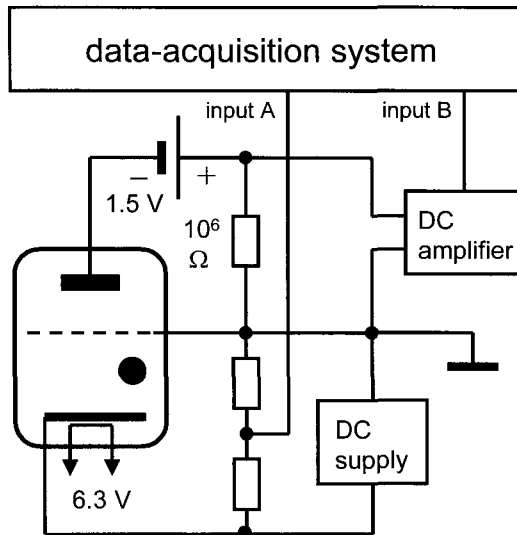


Fig. 2. Diagram of the setup with PHYWE's apparatus.

The apparatus includes a tube having a tungsten cathode and two additional electrodes, a grid and an anode. After pumping out, the tube is filled with a small amount of mercury and sealed. The tube is positioned in an electrically heated furnace. The density of the mercury vapor strongly depends on the temperature. The appropriate density is achievable by changing the temperature, which is measured with a thermocouple. The electrons emitted by the cathode are accelerated by a DC voltage and undergo collisions with the mercury atoms. With a battery, the potential of the anode is set to be 1.5 V lower than that of the grid. Therefore, the electrons that lose their energy due to inelastic collisions cannot arrive at the anode. The anode current is measured through the voltage drop across a $1\text{-M}\Omega$ resistor. A DC amplifier amplifies this voltage, which is then acquired by the data-acquisition system. Simultaneously, the system measures a definite part of the accelerating voltage (voltages above 10 V are dangerous for the inputs of our data-acquisition system). In the experiment, the I - U characteristic of the tube is measured and displayed automatically during the change of the accelerating voltage (Fig. 3).

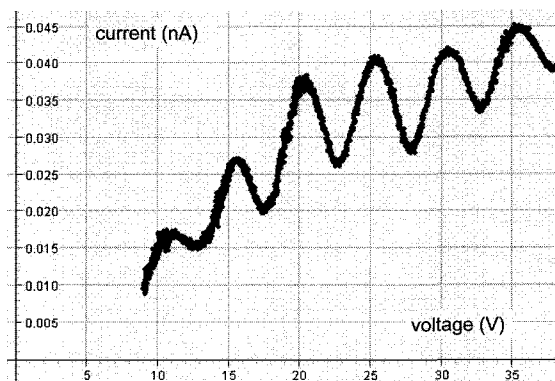


Fig. 3. Example of data obtained. The distance between neighbouring maxima or minima equals 4.9 V, the energy of the first excited state of mercury atoms.

The excitation and ionization potentials

A common thyratron, a gas-filled triode with a hot cathode, is used in another version of the Franck–Hertz experiment (Kraftmakher 1959a; Iveronova 1962). The thyratron contains a rare gas – argon, krypton or xenon (or their mixture). One gradually changes the accelerating voltage applied between the cathode and the grid and measures the grid and the collector currents (Fig. 4).

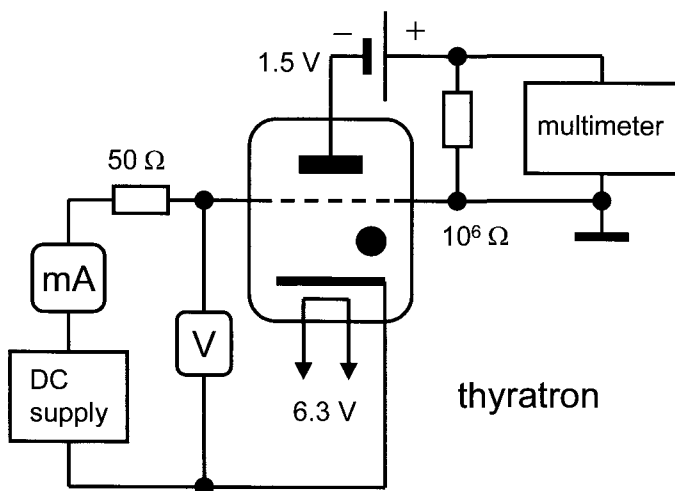


Fig. 4. Diagram of the setup with a thyratron.

With a battery, the potential of the collector is 1.5 V lower than that of the cathode, so that the energy of the emitted electrons is insufficient to overcome this barrier. The collisions of the emitted electrons with the atoms of the gas remain elastic until their energy amounts to that of the first excited level of the atom. When the excitation occurs, the excited atoms drop back to the initial state and emit photons. These photons cause photoelectric effect on the collector, which is seen from the voltage drop across a $1\text{-M}\Omega$ resistor put in the anode circuit. The appearance of the collector current unambiguously indicates the first excitation potential of the atoms of the gas (Fig. 5).

The ionization potential of the atoms of the gas is determined by measurements of the grid current. The current monotonically increases with the accelerating voltage, but it rises dramatically when positive ions appear in the thyratron. The ions travel to the cathode causing an increase of the electric field accelerating the emitted electrons. The ionization potential is therefore seen from the rise of the grid current. The current is measured by a milliammeter. To shield the grid from high currents, a $50\text{-}\Omega$ resistor is put in series with it. Both excitation and ionization potentials are thus determined. The measurements are possible with a data-acquisition system.

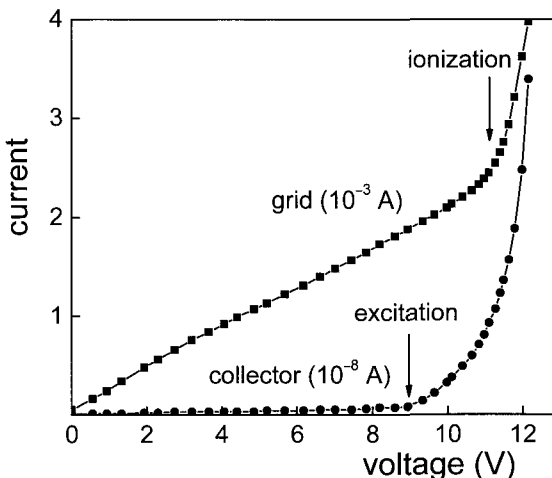
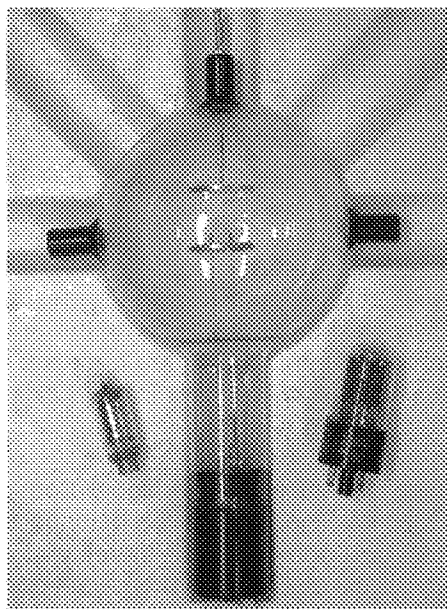


Fig. 5. Determination of the excitation and ionization potentials.

6.6. Thermionic emission

The experiments include the following topics: (i) thermionic emission and the work function; (ii) I - U characteristics of a vacuum diode; (iii) temperature of electrons emitted by a cathode; and (iv) calorimetric determination of the work function (Kraftmakher 1959a, 1998b).

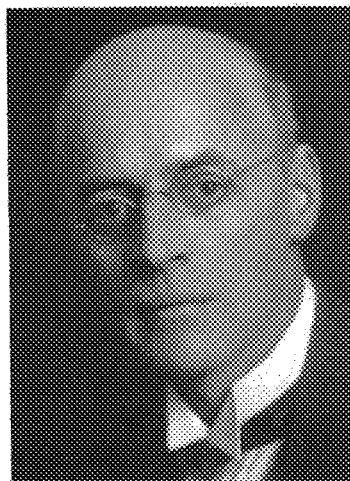


Vacuum diode from Leybold–Heraeus and other vacuum tubes used in the experiments.

Additional equipment:

Two *Voltage sensors*, vacuum tubes, DC supplies, function generator, variable resistor, decade resistance box (1 to 1000 Ω), multimeters, resistors, 9-V battery.

© The Nobel Foundation
Owen Willans Richardson
(1879–1959)



“...Professor Richardson. You are a happy man. You possess the very thing that gives life its chief value. You can devote yourself with all your strength to the activity that you love. We constantly see the results of this activity come to light. Besides this, you are fortunate enough to see the harvest ripen to the benefit of mankind in the fields you tilled in your youth.”

O. W. Oseen, member of the Nobel Committee for Physics. Presentation of Owen Willans Richardson awarded the Nobel Prize “for his work on the thermionic phenomenon and especially for the discovery of the law named after him” (1928).

What is worth remembering

The above formula “for the discovery of the law named after him” offers you an excellent idea how to get a Nobel Prize laureate. It is worth remembering, in this connection, discoveries bearing the names of the laureates: Röntgen rays (1901), Zeeman effect (1902), Wien law (1911), Planck formula (1918), Bohr theory (1922), Compton effect (1927), Wilson chamber (1927), Raman effect (1930), Heisenberg principle (1932), Dirac equation (1933), Pauli principle (1945), Cherenkov effect (1958), Mössbauer effect (1961), Néel point (1970), BCS theory (1972), Josephson effect (1973), Abrikosov vortices (2003).

Da liegt der Hund begraben!

Thermionic emission is of primary importance with vacuum tubes, electron microscopes, and other devices depending on a continuous supply of electrons. The discovery and studies of this phenomenon played an important role in the development of modern physics. Thomas Alva Edison (1847–1931) was probably the first to discover that negative electricity escapes from a hot filament (1883). In 1897, Joseph John Thomson established that the charge carriers are very small compared to the hydrogen ion. This was the electron. In 1900, Paul Drude (1863–1906) suggested that electrons are the carriers of current in metals, and Thomson proposed that they are also the negative charges emitted by hot metals. Owen Willans Richardson made a study on this basis (1901) and derived equations relating the current density to the absolute temperature. In 1925, Richardson used the new Drude's theory for explaining the emission in terms of the work function φ . The work function is the basic concept related to thermionic emission and the photoelectric effect. This quantity is defined as the energy difference between the Fermi level and the energy at a point in a field-free space outside the conductor (Fig. 1). Four basic methods are known for the determination of the work function: the Richardson method, the photoemission threshold, the contact potential difference, and the calorimetric technique (Herring and Nichols 1949; Craig 1975; Swanson and Davis 1985).

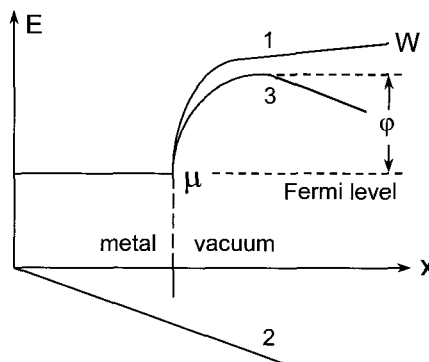


Fig. 1. Work function and Schottky's effect: 1 – energy barrier at zero external field, 2 – potential of the field, 3 – resulting energy barrier.

To be emitted, the electrons must have sufficient energy, directed in the positive x direction, to overcome the barrier $W = \mu + \varphi$. Assuming that all of the electron's energy is kinetic, this condition may be stated as $mv^2/2 > \mu + \varphi$, (1)

where m is the mass of the electron, v_x is the velocity component along the positive x direction, and μ is the Fermi level, the maximum electron energy in a metal at the absolute zero temperature. It was shown by Schottky that an external electric field E reduces the work function by

$$\Delta\varphi = -e^{3/2}E^{1/2}. \quad (2)$$

The problem is calculating the number of electrons that have the required velocities. The result is the so-called Richardson–Dushman equation for the thermionic current density:

$$j = (4\pi emk_B^2/h^3)T^2 \exp(-\varphi/k_B T) = AT^2 \exp(-\varphi/k_B T), \quad (3)$$

where e is the electron charge, k_B is Boltzmann's constant, T is the absolute temperature, and h is Planck's constant. The evaluation gives $A = 120 \text{ A.cm}^{-2}.\text{K}^{-2}$. Experimental values of φ and A for a number of metals and for monomolecular films on tungsten are given in Table 1.

Table 1. Parameters of thermionic emission φ (eV) and A ($\text{A.cm}^{-2}.\text{K}^{-2}$).

Metal	φ	A	Film	φ	A
Cs	1.81	162	Cs on W	1.36	3.2
Ba	2.11	60	Cs on O on W	0.72	0.003
Mo	4.15	55	Ba on W	1.56	1.5
W	4.54	60–100	Ba on O on W	1.34	0.18
Pt	5.40	170			

The simplest vacuum tube is the diode comprising a cathode and an anode. Three ranges of the I – U characteristic can be distinguished according to the potential U , at which the anode is held with respect to the cathode. The saturation current is obtained if a sufficient positive potential is applied to the anode, so that all the emitted electrons are collected. At voltages below that required for saturation, the repulsion between the electrons tends to limit the current. In this region, the current is proportional to $U^{3/2}$ (the Child–Langmuir law, or the so-called " $^{3/2}$ law"). For coaxial cathode and anode, the anode current is given by

$$I_a = 4A(e/m)^{1/2}\epsilon_0 U^{3/2}/(3r\beta)^2 = KU^{3/2}, \quad (4)$$

where A is the area of the cathode surface, ϵ_0 is the permittivity constant, r is the anode radius, and β is a geometrical correction constant (for the case of parallel-plane electrodes see Umstattd *et al.* 2005).

When the applied voltage is reversed so as to become retarding for electrons, the current is limited by the number of electrons with energy sufficient to overcome the retarding potential:

$$I = I_0 \exp(-eU/k_B T). \quad (5)$$

This expression is valid for the plane geometry of the electrodes. The temperature relates to the gas of electrons emitted by the cathode, and it equals the cathode temperature.

Vacuum tubes have now a very limited practical use, but they provide an excellent opportunity to teach some fundamental physical phenomena such as thermionic emission, the velocity distribution of electrons emitted, the Child–Langmuir law, and the Schottky effect. Corresponding experiments are included in many laboratory manuals. From time to time, papers appear describing variants of such student experiments. Brody and Singer (1970) determined the e/m ratio for the electron and the work function of tungsten. Dodd (1971) reported on an experiment, in which the cathode temperature was deduced from the energy distribution of the emitted electrons. Luke (1974) described an experiment including several aspects of thermionic emission. Knudsen (1985) compared the temperature of the emitted electrons with the cathode temperature measured with an optical pyrometer. Using a commercially available vacuum diode with a tungsten cathode, Greenslade (1991) determined the work function of tungsten. Wagner and Soonpaa (1994) developed a picoammeter for thermionic emission measurements over a wide range of currents.

Richardson's method

A vacuum diode with a tungsten cathode of direct heating (Leybold–Heraeus, catalog index 55507) is employed for the measurement of the thermionic current and the evaluation of the work function (Fig. 2). To reduce the influence of the voltage drop across the cathode, the anode circuit is connected to the middle point of a resistor R_1 shunting the cathode. Since a voltage fed to the inputs of our data-acquisition system must be below 10 V, the voltage applied to the anode is measured using a voltage divider. The anode current is determined through the voltage across a resistor R_2 connected in series with the diode. This voltage is amplified by a DC amplifier, Keithley 177 model multimeter, and then fed to the input of the data-acquisition system. The current heating the cathode is determined through the voltage drop across a resistor $R_3 = 0.1 \Omega$. It is easy to see that the steady-state temperature of a wire heated

by a current I_h in vacuum depends on the quantity $I_h/d^{3/2}$, where d is the diameter of the wire. When a current I_h is passed through a wire of length l , the electric power dissipated in it equals

$$P = 4I_h^2 \rho l / \pi d^2, \quad (6)$$

where ρ is the resistivity of the wire. In vacuum, this power is balanced by thermal radiation given by the Stefan–Boltzmann law:

$$P = \varepsilon \sigma \pi l d T^4, \quad (7)$$

where ε is the hemispherical total emittance of the sample, and σ is the Stefan–Boltzmann constant. From the above relations,

$$T^4 = 4I_h^2 \rho / \pi^2 \varepsilon \sigma d^3. \quad (8)$$

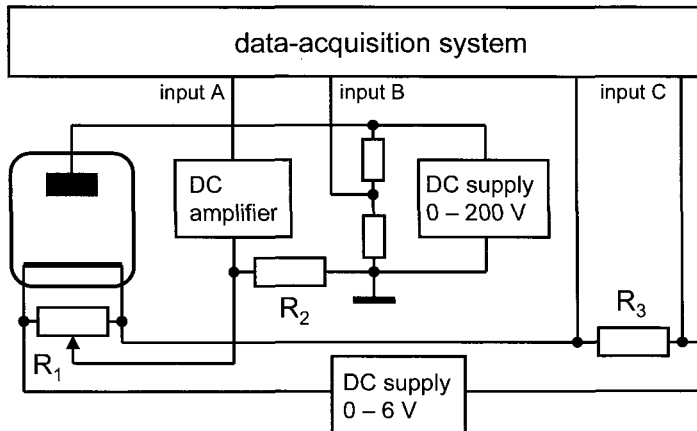


Fig. 2. Diagram of the setup for measuring thermionic currents.

The parameters ρ and ε and their temperature dependences are specific for different metals. For any given temperature, Eq. (8) contains only one variable parameter, the I_h^2/d^3 ratio. The steady temperature of a tungsten wire is a known function of this ratio, or of the ratio $X = I_h/d^{3/2}$. The data for tungsten presented in Table 2 allow one to calculate the temperature of a tungsten cathode from its diameter (cm) and the heating current (A). For these units, the polynomial fit to the dependence $T(X)$ is

$$T = 790 + 1.3 \times X - 1.2 \times 10^{-4} \times X^2. \quad (9)$$

To use this relation, one has to somehow determine the diameter of the cathode. The knowledge of real temperatures of tungsten cathodes is also useful for the estimation of the diameter. In our case, it was taken as 0.15 mm. Now the temperatures of the cathode can be calculated for any

heating current. In the first experiment, the anode current is measured, for several temperatures of the cathode, as a function of the anode voltage (Fig. 3). Then the saturation current, under the maximum anode voltage, is determined as a function of the heating current (Fig. 4).

Table 2. Temperature of a long tungsten wire in vacuum as a function of its diameter d (cm) and heating current I (A).

$I/d^{3/2}$ (A.cm $^{-3/2}$)	T (K)	$I/d^{3/2}$ (A.cm $^{-3/2}$)	T (K)
581	1500	1217	2200
662	1600	1319	2300
747	1700	1422	2400
836	1800	1526	2500
927	1900	1632	2600
1022	2000	1741	2700
1119	2100	1849	2800

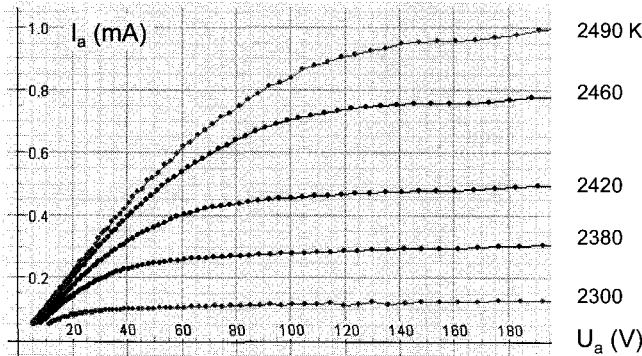


Fig. 3. I - U characteristics of a vacuum diode for various cathode temperatures.

Using Eq. (9), one translates the heating currents into temperatures of the cathode. According to Eq. (2), a plot of $\log(I_a/T^2)$ versus $1/T$ should be a linear graph ('Richardson's line'), from which the work function of tungsten is available (Fig. 5).

Due to the large diameter of the cathode, temperatures of its end parts are much lower than those of the center. There exist two ways to avoid or greatly reduce the influence of this effect. First, diodes with thinner cathodes should be used. Second, the currents from the ends of the cathode could be excluded with a special design of the diode. The

diode contains three cylinder anodes, which are kept at the same potential but the current through the central anode is only measured (Fig. 6).

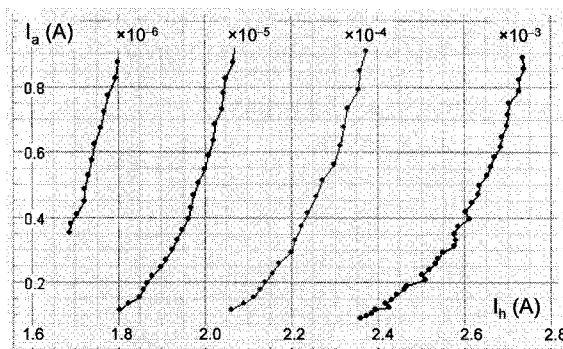


Fig. 4. Saturation current versus the current heating the cathode.

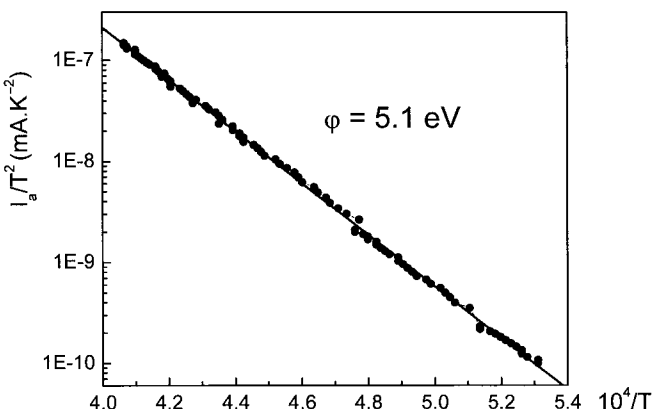


Fig. 5. ‘Richardson’s line’ that combines all the data provides the work function. The result is about 10% higher than the correct value.

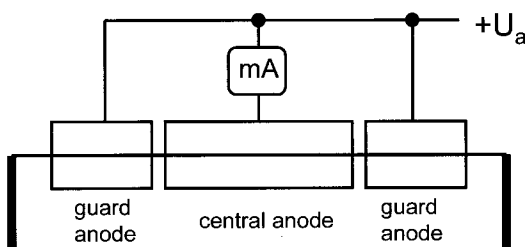


Fig. 6. Design of a vacuum diode with guard anodes.

Several decades ago, such a diode was commercially available (GRD7, the Ferranti guard ring diode). Diodes with such guard anodes can be manufactured when the necessary facility is accessible.

Temperature of emitted electrons

Another setup is used for the measurements at negative anode voltages. A vacuum diode with an oxide-coated cathode of indirect heating is employed for this purpose (Fig. 7).

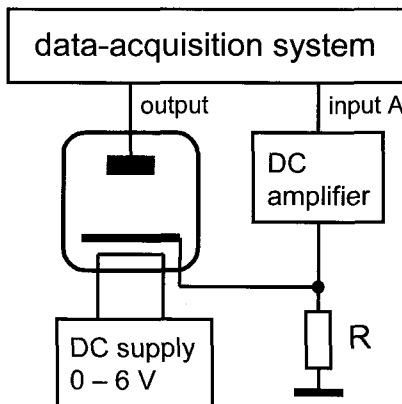


Fig. 7. Diagram of the setup for the determination of the temperature of emitted electrons.

The load resistor of the diode R can be set to be 10^2 , 10^3 , 10^4 , or $10^5 \Omega$. In our case, a decade resistance box (PASCO, PI-9588) serves as the load. The voltage across it is amplified by the Keithley 177 model multimeter and then fed to the input of the data-acquisition system. With the 20-mV scale, the multimeter provides a 100-fold amplification. A 0.001-Hz sine voltage from the *Signal generator* is applied to the diode. After switching the generator on, it starts to reproduce the negative part of the waveform. Then one observes the readout of the multimeter and starts the measurements when the voltage measured falls below 10 mV. When this voltage achieves 1 mV, one changes the load resistor. These measurements repeated for all the load resistors provide data over a wide range of anode currents, from 10^{-8} to 10^{-4} A (Fig. 8).

The low-current part of the $I-U$ characteristic obeys Eq. (5), so the dependence of $\log I_a$ versus U is a straight line. The decrease of the slope at higher currents means the transition to the space-charge-limited

region. The transition point differs from the zero voltage because of the contact potential difference between the cathode and anode. The measurements of the characteristics are done for two regimes of heating the cathode: 6 V (0.6 A) and 4 V (0.46 A). From the graphs (Fig. 9), the temperatures of the electrons emitted by the cathode are available.

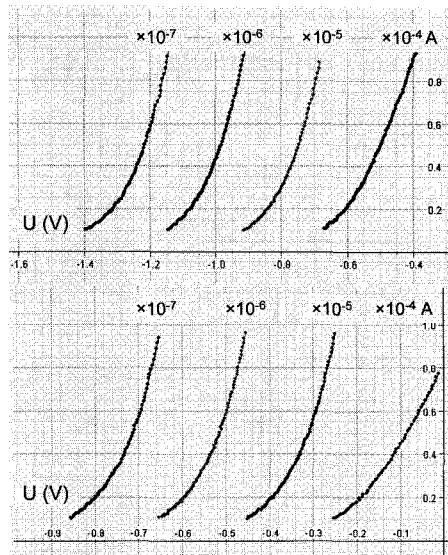


Fig. 8. I - U characteristics of the vacuum diode at negative anode voltages, for two voltages applied to the cathode heater, 6 V and 4 V.

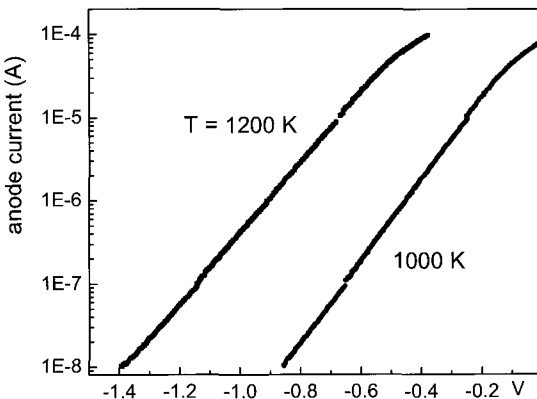


Fig. 9. Graphs of $\log I_a$ versus U . From the straight parts of the graphs, the temperatures of the electron gas equal 1200 and 1000 K, which are reasonable values for oxide-coated cathodes.

Calorimetric determination of the work function

This experiment clearly demonstrates the energy transfer by electrons leaving a cathode of a vacuum tube. Oxide-coated cathodes are more suitable for such measurements than tungsten cathodes (Kraftmakher 1959a, 1998b). Among other methods, the calorimetric technique is used very rarely and is not even mentioned in many textbooks. Probably one of the last such measurements was reported by Fleming and Henderson (1940). However, a direct measurement of the work function according to its definition deserves attention. The calorimetric method makes use of the cooling of the cathode due to the emission of electrons. The theory of this phenomenon is very simple. Every electron leaving the cathode takes away energy equal to $\varphi + 2k_B(T - T_0)$, where T is the temperature of the cathode, and T_0 is room temperature. The second term is due to initial velocities of the emitted electrons that leave the cathode at a high temperature and return to it at room temperature. The term $2k_B T$ differs from the mean thermal energy because the energy transfer depends also on the velocity of the emitted electrons in a given direction. This term is one order of magnitude smaller than the work function, so there is no need to precisely determine the temperature of the cathode.

When a current I_a flows through a vacuum tube, the number of electrons leaving the cathode per second is I_a/e . When the anode circuit is disconnected, the emitted electrons form a space charge around the cathode and equilibrium is set up between the emitted electrons and those returning to the cathode. After closing the anode circuit, a steady current flows through the tube, causing the cooling of the cathode (Fig. 10). The energy transfer by the emitted electrons per second is given by

$$\Delta P = [\varphi + 2k_B(T - T_0)]I_a/e. \quad (10)$$

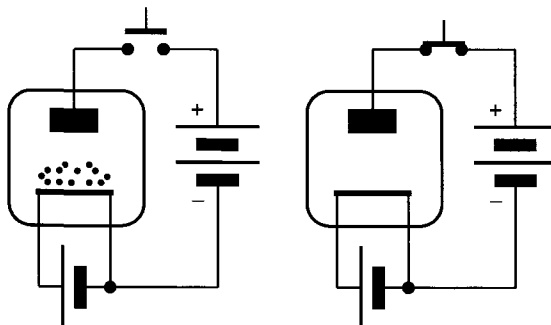


Fig. 10. Vacuum tube with an open and closed anode circuit.

This power amounts to only a small part of the total heat loss from the cathode, which is mainly due to thermal radiation. However, it is measurable. To estimate the expected results, it is useful to consider the ratio of the thermionic current to the power heating the cathode. Since both quantities are proportional to the cathode's area, this ratio depends only on the temperature and the parameters of the thermionic emission. This quantity can be considered as the efficiency of a cathode. The thermionic current grows with temperature more rapidly than the heating power. The efficiency thus increases with temperature, being $10\text{--}100 \text{ mA.W}^{-1}$ for oxide-coated cathodes and $0.1\text{--}1 \text{ mA.W}^{-1}$ for tungsten cathodes. The main part of the energy transfer per second is equal to the product of the anode current and the work function expressed in electron volts. The expected relative contributions to the heat loss thus range from 1.5% to 15% for oxide-coated cathodes ($\varphi = 1.5 \text{ eV}$) and from 0.05% to 0.5% for tungsten cathodes (4.5 eV).

A compensation technique is applicable in the measurements: one balances the energy transfer by properly changing the current heating the cathode. Therefore, there is no need for measuring the temperature drop caused by the energy transfer. However, it is easy to estimate this drop. Under radiation heat transfer, the power necessary to heat the cathode is proportional to T^4 , and a simple relation holds: $\Delta P/P = 4\Delta T/T$ ($\Delta T \ll T$). From this relation, the temperature drop is expected to be 6 to 60 K for an oxide-coated cathode and 0.3 to 3 K for a tungsten cathode. More rigorously, one has to take into account the temperature dependence of the total emittance of the cathode, which makes the temperature dependence of the heating power somewhat stronger and the expected temperature drop smaller. The above estimates show that oxide-coated cathodes are much more favorable for calorimetric determinations of the work function than tungsten cathodes.

- *Oxide-coated cathode.* Any vacuum tube with an oxide-coated cathode of direct heating is suitable for the measurements. Thin cathode filaments, *i.e.*, of low heating current, are preferable. In our case, the vacuum tube CV 1758/1L4 (a pentode) is employed. Its control and screen grids are connected to the anode. The cathode is included in a bridge circuit (Fig. 11) fed by a DC supply operating in the constant-current mode, *i.e.*, the current is independent of the load resistance. The output voltage of the bridge is amplified by the Keithley model 177 multimeter and then fed to the data-acquisition system. The anode of the vacuum tube is connected to a 9-V battery through a switch. The second terminal of the battery is connected to a middle point of a potentiometer shunting the cathode. This is done in order to reduce the influence of the additional voltage drop across the cathode caused by the current through

the tube. The resistance of the potentiometer is $2\text{ k}\Omega$, two orders of magnitude larger than that of the cathode.

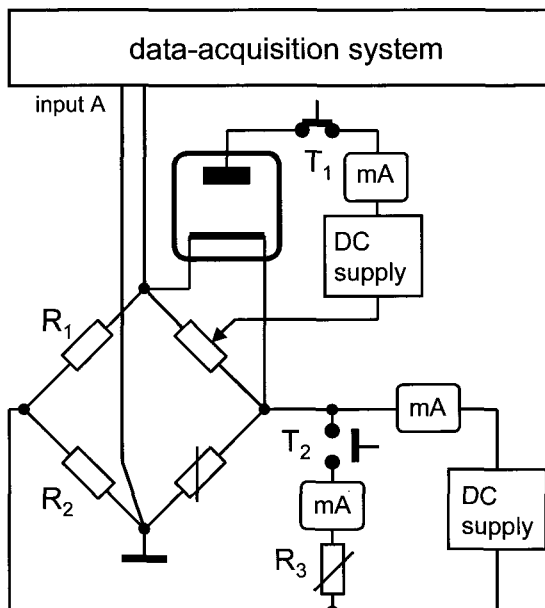


Fig. 11. Circuit for calorimetric determinations of the work function. $R_3 = 5\text{ k}\Omega$.

A variable resistor R_3 and a milliammeter form an auxiliary circuit producing adjustable and readily measurable changes in the current heating the cathode. This circuit is connected in parallel to the bridge through the second pair of contacts of the switch. These contacts are closed when the first pair is broken and vice versa. Therefore, when the anode circuit is disconnected and the temperature of the cathode is increased, the auxiliary circuit takes away part of the heating power. Since the DC supply operates in the constant-current mode, the decrease in the current feeding the bridge is exactly equal to the current through the auxiliary circuit. The power heating the cathode decreases by $2RI_h\Delta I_h$, where R is the resistance of the cathode, I_h is the heating current, and ΔI_h is its small decrease. The current through the parallel circuit is adjusted to restore the initial resistance (*i.e.*, the initial temperature) of the cathode. Hence,

$$\varphi = 2eRI_h\Delta I_h/I_a - 2k_B(T - T_0). \quad (11)$$

In the bridge, $R_1 = 10\text{ }\Omega$, $R_2 = 1\text{ k}\Omega$, and there is no need to take into account the distribution of the feeding current in the arms of the

bridge. The measurements are performed with anode currents from 1 to 5 mA. The work function is calculated as an average of the results obtained for both directions of the heating current. The position of the slide of the potentiometer R_3 should be set in such a way that the difference between the two results is reduced to a minimum.

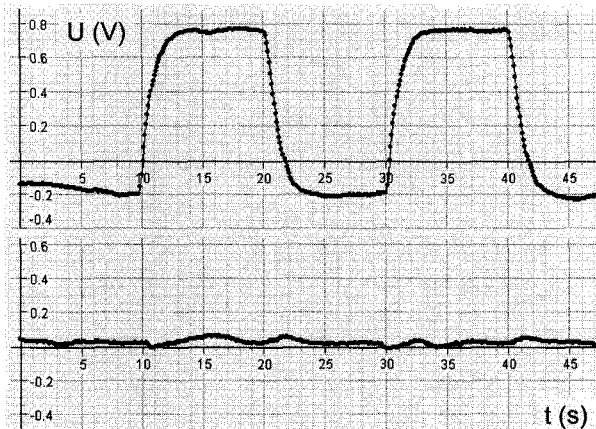


Fig. 12. Output voltage (after 100-fold amplification) when switching the anode current (1 mA) on and off, before and after the compensation.

The energy transfer by emitted electrons can be easily seen when the current through the tube is periodically interrupted and the output voltage of the bridge is recorded (Fig. 12). The temperature of oxide-coated cathodes is in the range 1200–1800 K. The quantity $2k_B(T - T_0)$ thus is 0.2 ± 0.05 eV. The residual uncertainty is of minor significance. The temperature dependence of the work function of an oxide-coated cathode may be expressed as $\phi = \phi_0 + \alpha T$. For a mixture of BaO and SrO, values of $\phi_0 \approx 1$ eV and $\alpha \approx 6 \times 10^{-4} T$ eV.K⁻¹ were recommended by Craig (1975). The results obtained are in reasonable agreement with this fit (Fig. 13). It is worth remembering that Richardson's method is hardly applicable to oxide-coated cathodes because they manifest no saturation current, due to the strong dependence of the work function on the electric field on the cathode surface.

- *Tungsten cathode.* The only vacuum tube with a tungsten cathode available to us is the diode from Leybold–Heraeus, catalog index 55507. The same bridge circuit was employed for the measurements, but with $R_1 = 1 \Omega$ (25 W), $R_2 = 100 \Omega$, and $R_3 = 200 \Omega$. For tungsten cathodes, the quantity $2k_B(T - T_0)$ can be taken as 0.4 ± 0.05 eV. The determined value of the work function, 5.3 ± 0.3 eV, is markedly above

the expected one, 4.5 eV. Greenslade (1991) reported a similarly high value from Richardson's plot. He explained the increase in the work function by a surface contamination. In our case, it may be partly caused by the resistance of long current leads inside the tube and by the influence of the cold portions of the cathode adjacent to the leads. The length of these portions amounts to about 10% of the total length of the cathode. Thin cathodes should be used to reduce this effect. To check the above assumption, the measurements were carried out with a thin tungsten filament. A light bulb (12 V, 10 W) was employed. After removing the glass envelope, it was placed in a vacuum chamber providing vacuum of about 10^{-4} Pa. An additional electrode mounted close to the filament served as the anode. The same bridge was used as in the measurements with the oxide-coated cathode. For this filament, the work function appeared to be close to the true value.

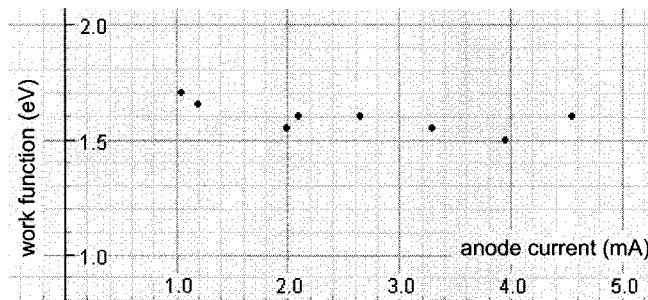
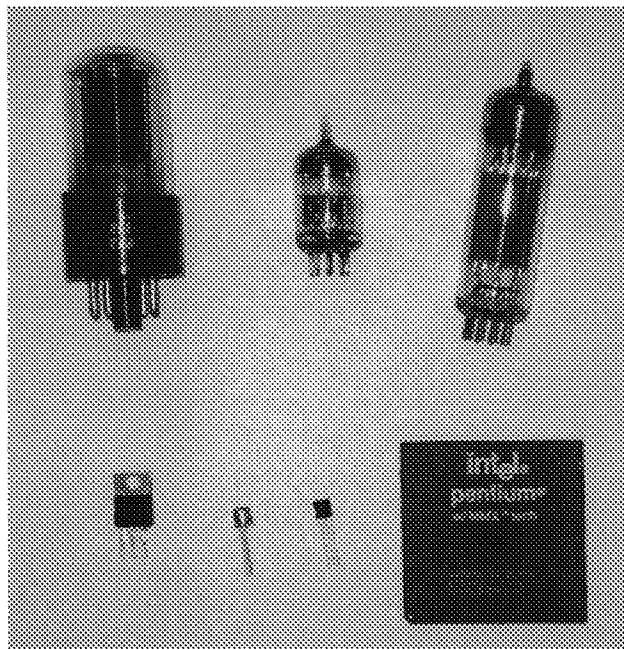


Fig. 13. The work function measured with various anode currents. The mean value is about 1.6 eV.

The experiments presented were included in many laboratory courses (Iveronova 1962, 1968; Portis 1964, 1972; Soloukhin 1975; Goldin 1983). Some of them were described by the author (Kraftmakher 1959a, 1959b, 1961, 1998b).

6.7. Transistor

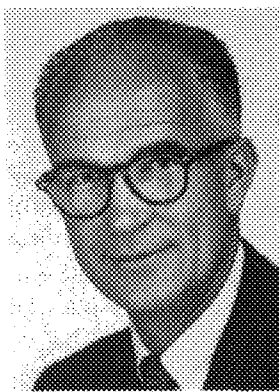
I-U characteristics of a bipolar junction transistor and of a junction field-effect transistor are displayed with a data-acquisition system. The operation of a transistor amplifier is monitored with an oscilloscope.



Vacuum electron tubes, transistors, and a microprocessor containing several million transistors.

Additional equipment:

Voltage sensor, Power amplifier II, transistors, DC supply, multimeter, oscilloscope, function generator, decade resistor box.



© The Nobel Foundation
William Shockley
(1910–1989)



© The Nobel Foundation
John Bardeen
(1908–1991)



© The Nobel Foundation
Walter Houser Brattain
(1902–1987)

“...Doctor Shockley. Doctor Bardeen. Doctor Brattain. The summit of Everest was reached by a small party of ardent climbers. Working from an advance base, they succeeded. More than a generation of mountaineers had toiled to establish that base. Your assault on the semiconductor problem was likewise launched from a high-altitude camp, contributed by many scientists. Yours, too, was a supreme effort – of foresight, ingenuity and perseverance, exercised individually and as a team. Surely, supreme joy befalls the man to whom those breathtaking vistas from the summit unfold.”

E. G. Rudberg, member of the Nobel Committee for Physics.
Presentation of William Shockley, John Bardeen, and Walter Houser Brattain awarded the Nobel Prize “for their researches on semiconductors and their discovery of the transistor effect” (1956).

With a data-acquisition system, it is easy to display characteristics of a device such as a transistor or an amplifier. The *Signal generator* incorporated into the *ScienceWorkshop 750 Interface* serves as a source of necessary voltages. A DC power supply, a function generator, and an oscilloscope are also used in the measurements. Characteristics of a bipolar junction transistor 2N2222A and of a junction field-effect transistor 2N5461 are displayed by *DataStudio*. For an experiment very useful for understanding the transistor operation see Sconza and Torzo (1987).

Bipolar junction transistors

Bipolar junction transistors are three-layer devices, basically either *p-n-p* or *n-p-n* sandwiches (Fig. 1). Both types function in the same manner, although potentials and charges will have opposite polarities in the two cases. Several operating modes of a transistor may be considered (Beeforth and Goldsmid 1970; Li 1993; Balkanski and Wallis 2000). Suppose the base-emitter voltage V_{BE} applied to the base of an *n-p-n* transistor to be negative. Both the transistor junctions, collector-base and base-emitter, will be reverse-biased, and only the usual diode leakage current will flow through them. The transistor is said to be ‘off’.

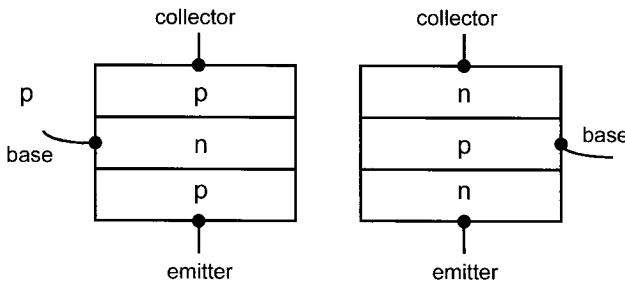


Fig. 1. Diagrams of *p-n-p* and *n-p-n* transistors.

Biasing the base positive with respect to the emitter will turn the transistor ‘on’. The emitter junction will be forward-biased, whereas the collector junction will still be reverse-biased. Usually, the emitter doping is made substantially heavier than the base doping, so that forward currents across the emitter-base junction are almost entirely due to carrier injection from emitter to base rather than from base to emitter. By having very narrow base widths, almost all the emitter-to-base I_E current will arrive at the collector junction and cross into the collector. The base current I_B equals to the net recombination rate of excess minority carriers within the base. The ratio I_C/I_B is usually denoted by β . Since $I_B = I_E - I_C$,

$$I_C = I_E\beta/(\beta + 1). \quad (1)$$

The input of the transistor may be considered either as a voltage V_{BE} , or as a current I_B . Using data acquisition, it is easy to observe $I-U$ characteristics of a transistor. The *Power amplifier II* provides a *Ramp up wave* collector-emitter voltage (Fig. 2). The base current is measured by the voltage drop across a $100\text{-}\Omega$ resistor, and the collector current as the output current of the amplifier. Both currents are stored and displayed versus the collector-emitter voltage. A battery or a DC supply provides

the base-collector voltage. The characteristics show the narrow range of the controlling voltage, the need for a bias, and the current gain (Fig. 3).

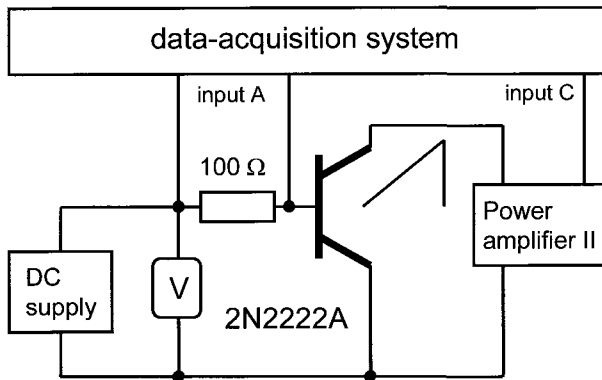


Fig. 2. Diagram of the setup for the measurements.

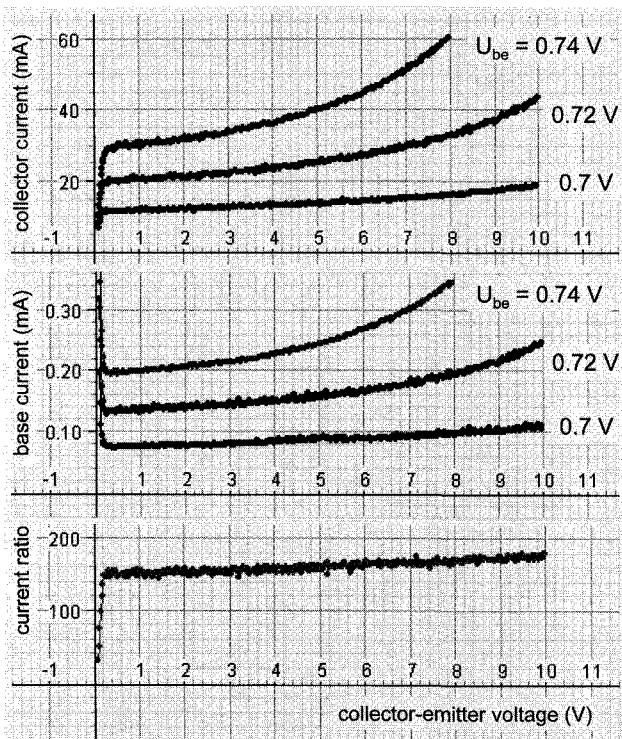


Fig. 3. Characteristics of a bipolar transistor 2N2222A.

Junction field-effect transistors

The junction field-effect transistor (JFET) is a three-terminal device consisting of a source, a gate, and a drain electrode (Fig. 4). The current flow through a channel between the source and drain electrodes is controlled by a voltage applied to the gate. The channel is formed between the gate and the substrate. If the current flow is due to electrons, we have an *n*-channel. The main feature of a JFET is that a reverse-bias gate voltage controls the width of the depletion layer in the *p*-gate and *n*-channel space-charge region and thus the conductivity of the channel.

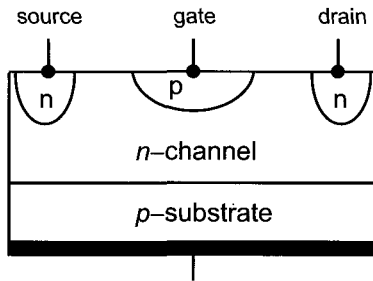


Fig. 4. Diagram of an *n*-channel junction field-effect transistor.

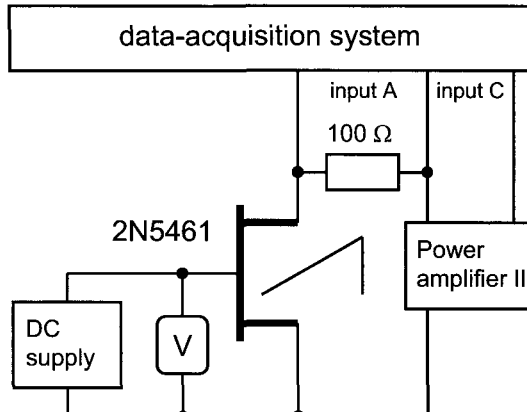


Fig. 5. Diagram of the setup for the measurements.

In the experiment, the *Power amplifier II* provides a voltage applied between the source and the drain of a JFET (Fig. 5). The voltage is stored as the *Output voltage* and the current is measured by the voltage across a $100\text{-}\Omega$ resistor. A regulated DC supply provides the gate voltage. *DataStudio* displays the *I-U* characteristics (Fig. 6).

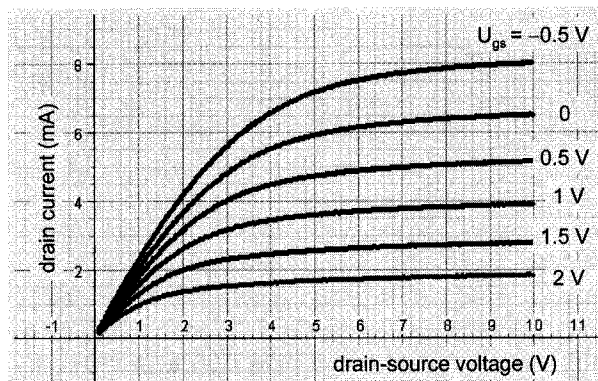


Fig. 6. Characteristics of a field-effect transistor 2N5461.

Transistor amplifier

A simple circuit with a field-effect transistor and an oscilloscope demonstrates the operation of a transistor amplifier. The transistor 2N5461 is loaded by a decade resistor box R (Fig. 7).

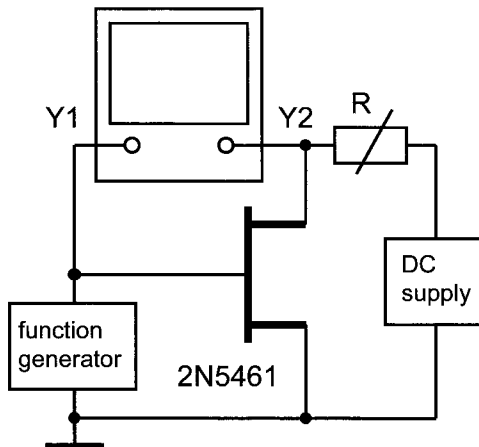


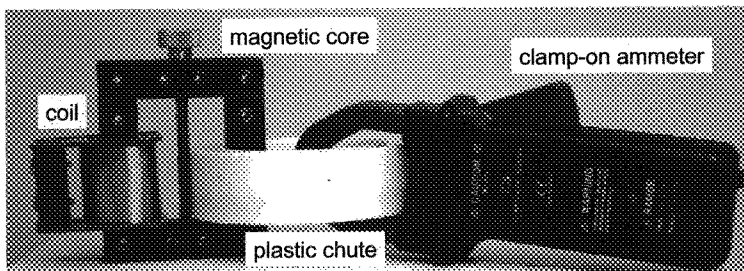
Fig. 7. Diagram of a single-stage amplifier with a field-effect transistor.

An AC voltage from a function generator is applied between its source and gate and monitored with an oscilloscope. The second input of the oscilloscope shows the voltage across the load, and it is easy to see the relation between the input and output voltages for different load

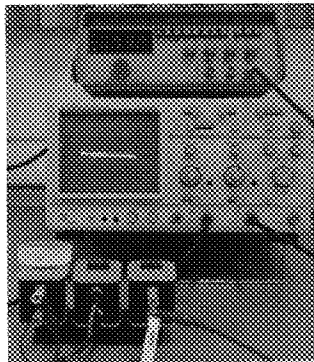
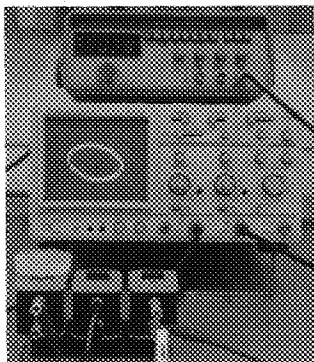
resistors. It is useful to display the relation between the two voltages as the Lissajous figure. In this case, the frequency dependence of the phase shift introduced by the amplifier becomes observable. The gain of the amplifier drops when increasing the frequency of the signal.

6.8. Superconductivity

The experiments include several topics: (i) zero resistivity; (ii) U - I characteristic and critical current at 77 K; (iii) magnetization curves and field dependence of the magnetic susceptibility; (iv) the phase transition to the superconducting state; and (v) diamagnetic properties of superconductors (Kraftmakher 1999, 2004e).



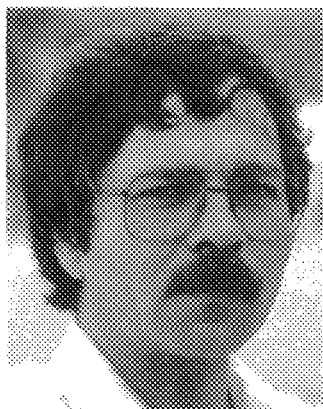
Contactless determinations of U - I curves of a superconducting ring.



Demonstration of the superconducting state.

Additional equipment:

Two *Voltage sensors*, YBCO and BSCCO-2223/Ag samples, lock-in amplifier, DC supply, DC amplifier, oscilloscope, Dewar flask, clamp-on ammeter, variac, isolation transformer, multimeter, platinum resistance thermometer, coils, laboratory jack, variable resistor, resistors, capacitor, dismountable transformer, 9-V battery.



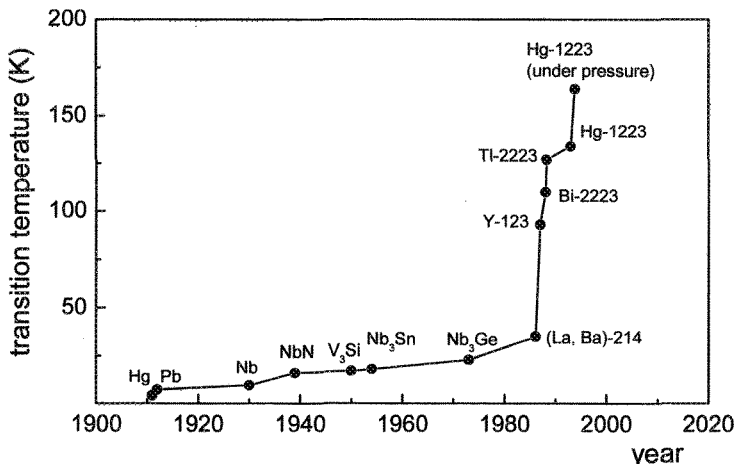
© The Nobel Foundation
J. Georg Bednorz



© The Nobel Foundation
K. Alexander Müller

"...This discovery is quite recent – less than two years old – but it has already stimulated research and development throughout the world to an unprecedented extent. The discovery made by this year's laureates concerns the transport of electricity without any resistance whatsoever and also the expulsion of magnetic flux from superconductors."

Gösta Ekspong, the Royal Academy of Sciences. Presentation of J. Georg Bednorz and K. Alexander Müller awarded the Nobel Prize "for their important breakthrough in the discovery of superconductivity in ceramic materials" (1987).



This diagram clearly shows the importance of the Bednorz–Müller discovery.

High-temperature superconductors provide an excellent opportunity for including superconductivity in student laboratory courses. This seems not to have been fully exploited until now, although many classroom demonstrations and laboratory experiments on superconductivity have been already reported. First such experiments were described even before the discovery of high-temperature superconductors. In most of the demonstrations, the interaction between a permanent magnet and a superconducting sample was shown (Early *et al.* 1988; Reich 1988; Oseguera *et al.* 1989; Ouseph 1989; Valenzuela *et al.* 1999). The temperature dependence of the resistivity of superconductors was measured in several classroom demonstrations and in laboratory experiments (Smith and Tinkham 1980; Kirkup 1988; Brown *et al.* 1989; Pechan and Horvath 1990; Vandervoort *et al.* 1995; León-Rossano 1997). Determination of the critical currents (Oldenburg *et al.* 1993) and observation of the diamagnetic screening (Lukefahr *et al.* 1997) were also used. In other student experiments, superconductivity was observed through changes in the resonance frequency of an *LC* circuit with a sample inside the inductor (Fox *et al.* 1988), by measurements of the persistent currents (Rowland 1975; Liu *et al.* 1990; Tiernan 1997), and of the AC magnetic susceptibility (Behroozi and King 1976; Behroozi 1983; Nicolo 1995; Nanda 1998). Ewert (1987) demonstrated the phase transition of a tantalum sample calorimetrically. Hegman *et al.* (1998) considered a superconducting pendulum as a thermodynamic machine.

Three experiments were described by the author (Kraftmakher 1999): (i) observation of the phase transition curves by means of a homemade magnetometer; (ii) determination of the influence of an external magnetic field on the magnetic susceptibility of a sample; and (iii) observation of magnetization curves. Later, two demonstrations on superconductivity were presented: (i) U - I curves and the critical current, and (ii) diamagnetic properties of superconductors (Kraftmakher 2004e).

Techniques known for contactless detection of superconductivity are the following:

- Samples in DC magnetic fields (the magnetic susceptibility, magnetization, the field shielding, and forces in nonuniform magnetic fields).
- Samples in AC magnetic fields (the real and imaginary parts of the magnetic susceptibility, the field shielding, and the torque caused by a rotating magnetic field).
- Persistent electric currents and the remanent magnetization of a superconducting sample.

Basic features of superconductors

Heike Kammerlingh-Onnes discovered superconductivity in 1911. This discovery became possible after liquefying helium, the last 'true' gas at low temperatures. For this achievement, Kammerlingh-Onnes was awarded the Nobel Prize (1913). In his Nobel lecture, the laureate drew attention also to a recently discovered phenomenon consisting of abruptly dropping the resistivity of mercury to zero at 4.1 K. The decrease of the resistivity of metals with decreasing temperature was well known, and Kammerlingh-Onnes intended to confirm such behavior at very low temperatures. Unexpectedly, he observed a sharp transition to a superconducting state at a certain critical temperature, with exactly zero resistivity (Fig. 1).



"...Thus the mercury at 4.2 K has entered a new state, which, owing to its particular electric properties, can be called the state of superconductivity."

H. Kammerlingh-Onnes, Nobel lecture.

© The Nobel Foundation
Heike Kammerlingh-Onnes
(1853–1926)

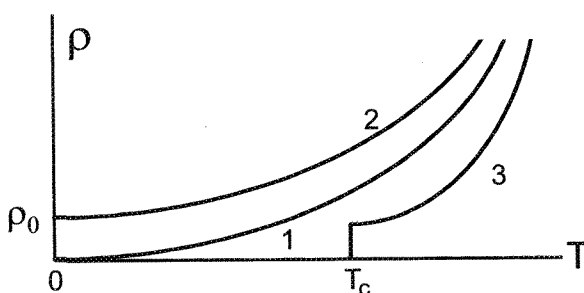


Fig. 1. Resistivity at low temperatures. 1 – resistivity of an ideal metal vanishes at absolute zero temperature, 2 – metal with impurities and structure defects manifests residual resistivity ρ_0 , 3 – resistivity of a superconductor disappears at a certain temperature.

In 1933, the second fundamental feature of superconductors was discovered by Meissner and Ochsenfeld. Superconductors appeared to be ideal diamagnets: persistent currents in a sample are sufficient to entirely compensate for, inside the sample, any external magnetic field. This means that the magnetic field inside a superconductor always equals zero. However, there exists an external field, the so-called critical field B_c , which destroys superconductivity. The critical magnetic field depends on temperature. The next very important point is the existence of superconductors of type I and of type II. They manifest different magnetic properties (Figs. 2 and 3).

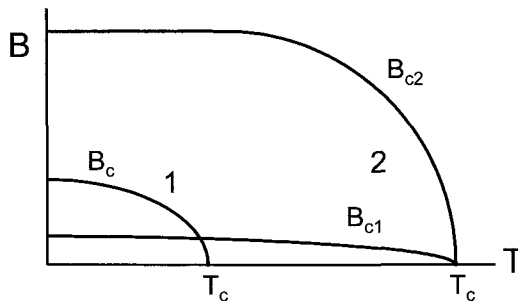


Fig. 2. Phase diagram of superconductors of type I (1) and of type II (2).
Superconductors of type II have two critical fields, B_{c1} and B_{c2} .

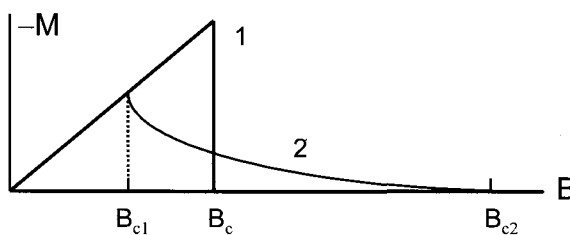


Fig. 3. Magnetization of superconductors of type I (1) and type II (2) in an external magnetic field.

High-temperature superconductivity

The phenomenon of superconductivity was indeed a challenge for physicists. In 1957, Bardeen, Cooper, and Schrieffer developed a theory of superconductivity, the so-called BCS theory (Nobel Prize, 1972). Superconductivity has great potential for applications in various fields (transformers, power transmission cables, electrical generators and motors, magnetic-levitated transport).

It is not surprising that great efforts were applied to synthesize superconductors having higher critical temperatures. A special term even appeared, ‘high-temperature superconductivity’. During many years, the critical temperature was enhanced up to about 23 K. At that time, the majority of the scientific community did not even believe that high-temperature superconductivity is feasible. Therefore, the discovery by Bednorz and Müller of a new class of superconductors possessing high critical temperatures (1986) was immediately recognized as one of the most important discoveries of the century (Nobel Prize, 1987). Many physicists, even those who never dealt with superconductivity, began to intensively work in this field. In a short time after the discovery, new superconductors of the same type (oxide cuprates) were found, and now the highest critical temperature under normal pressure is about 110 K. Even higher critical temperatures were achieved under high pressures. It is worth mentioning that the boiling point of nitrogen (77.4 K at normal pressure) is a crucial temperature point, above which a superconductor can be called a high-temperature superconductor from a practical point of view. This is due to the low cost and other advantages of using liquid nitrogen compared to liquid helium or other coolants providing lower temperatures.

Nowadays, superconducting tapes containing Bi-Sr-Ca-Cu-O filaments embedded in a metal matrix became available. Such tapes allow one to prepare stable superconducting samples. An Ag-sheathed multifilamentary $\text{Bi}_{2-x}\text{Pb}_x\text{Sr}_2\text{Ca}_2\text{Cu}_3\text{O}_{10}$ (BSCCO-2223/Ag) tape was purchased from the American Superconductor Corporation. According to the manufacturer, the transition temperature of this material is around 110 K. In some experiments described below, we use the tape 2.8 mm wide and 0.16 mm thick. The tape contains 55 superconducting filaments, whereas the fill factor of the tape is approximately 43%.

Resistance versus temperature

For the measurements, a piece of the BSCCO-2223/Ag tape equipped with potential probes is put, together with a small platinum thermometer, into a plasticine rod. The resistance of the thermometer is measured by a Keithley 177 model multimeter. The sample is fed by a DC supply (Fig. 4). After cooling in liquid nitrogen, the rod starts to warm up. The voltage between the potential probes is amplified by a DC amplifier and then stored, as well as the resistance of the platinum thermometer. *DataStudio* translates the resistance into temperature and displays the resistance of the sample versus temperature (Fig. 5).

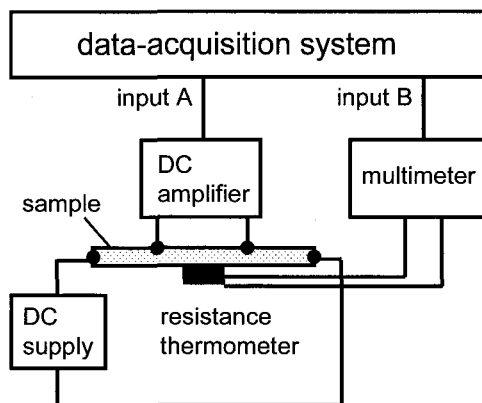


Fig. 4. Diagram of the setup for measuring electrical resistance of the sample.

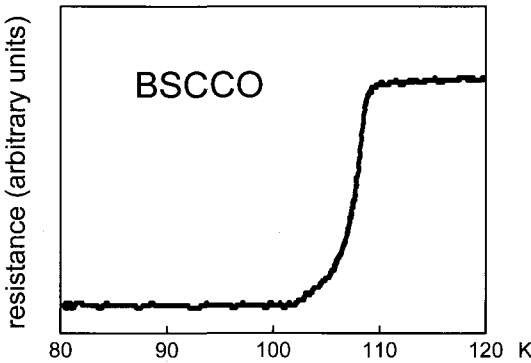


Fig. 5. Resistance of the BSCCO-2223/Ag sample versus temperature.

***U–I* characteristic and critical current**

A superconducting ring was prepared by soldering two ends of a piece of the BSCCO-2223/Ag tape. Its length is 35 cm, and the length of the overlapping parts of the tape is 4 cm. The soldering introduces small contact resistance, typically less than $10^{-7} \Omega$. It is easy to determine this resistance and to take it into account. The use of a short-circuited ring sample provides a very important advantage because large currents in it, of the order of 10^2 A, are obtainable with a low-power AC source. The well-known transformer method (e.g., González-Jorge *et al.* 2004) is used for obtaining the U – I curves of the ring. This technique is sufficiently simple to be reproduced in any student laboratory (Fig. 6).

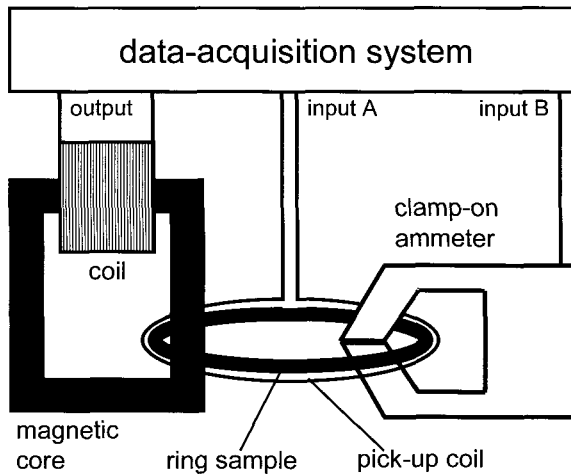


Fig. 6. Contactless determinations of U - I curves. A transformer generates an EMF in the ring, and a clamp-on ammeter measures the current.

The ring sample is placed in a plastic chute embracing the magnetic core of a demountable transformer and filled with liquid nitrogen. The chute retains liquid nitrogen for a short time, but quite sufficient to perform the measurements. The time of collecting the data is restricted by one period of the AC voltage generated in the ring. The sample rate of the data-acquisition system is set to obtain several hundred experimental points during one period of the voltage. When the frequency of the current is sufficiently low, the U - I characteristic is very similar to that obtainable by usual DC contact measurements.

A 1600-turn coil (PASCO, SF-8612) fed by the *Signal generator* constitutes the primary winding of an O-shaped demountable iron-core transformer (SF-8614). The ring sample forms the short-circuited secondary winding. A pick-up coil wrapped around the ring serves for measuring the voltage generated in the ring. When the same AC magnetic flux penetrates areas within the ring and the pick-up coil, the voltage generated in the coil strictly relates to that in the ring, according to the number of turns in the coil. Only a minor magnetic flux through an unavoidable small gap between the ring and the pick-up coil makes a contribution that is difficult to take into account. In our case, the pick-up coil contains ten turns and provides a voltage ten times larger than that generated in the ring. This voltage proceeds to the input of the data-acquisition system. A contactless clamp-on ammeter measures the current flowing in the ring and provides data for the second input of the data-acquisition system. The meter provides an output voltage

proportional to the current in the sample. The sensitivity of our meter is 10 mV.A^{-1} .

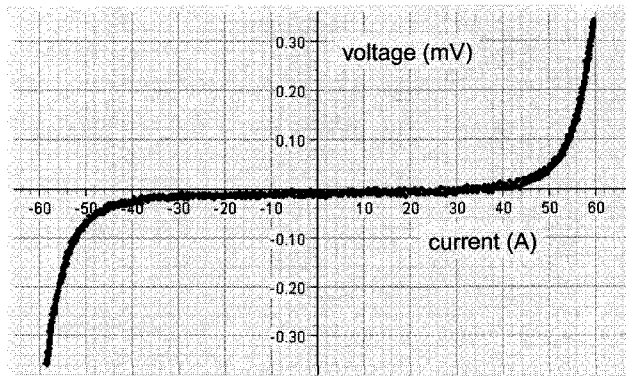


Fig. 7. U - I characteristic of the ring. The slope of the characteristic at low currents is caused by the resistance of the joint point.

The U - I characteristic (Fig. 7) was obtained with a 0.1-Hz current in the primary winding. The characteristic clearly shows a sharp increase in the voltage necessary to be generated in the ring when the current exceeds a definite critical value. According to a widely accepted criterion, the critical current is the current flowing when the electric field in a sample amounts to $1 \mu\text{V.cm}^{-1}$. A small constant slope of the U - I characteristic of our ring at currents lower than the critical current is due to the resistance of the joint point. In the vicinity of the critical value, the characteristic follows a power-law dependence, $U = AI^n$ (Carr 2001). The better the homogeneity of the sample, the larger the power index n , and the sharper the U - I dependence. The critical current of the ring, according to the above criterion, amounts to about 50 A. This means that the critical current density of the sample equals 10^4 A.cm^{-2} , which is about 20 times larger than that for usual copper wires.

Magnetization curves

A differential transformer serves for observing the magnetization curves of a superconductor in AC magnetic fields. Helmholtz coils constitute the primary winding of the transformer (Fig. 8). A variac and an isolation transformer, which is necessary for safety (not shown in Fig. 8), feed primary coils L_1 and L_2 . Resistors R_1 and R_2 , 0.1Ω each, are connected in series with the primary winding and provide a voltage for one input of

the data-acquisition system. Two similar secondary coils L_3 and L_4 are positioned inside a Dewar flask filled with liquid nitrogen. They are connected in opposition, so that in the absence of a sample the output voltage of the transformer is zero. Each secondary coil, 2 cm in diameter and 2 cm long, contains 5000 turns. To finely balance the transformer, a small additional coil (not shown in Fig. 8) is connected in series with the secondary coils. This coil is placed near the Helmholtz coils, and its position is chosen to null the background voltage. The quadrature component of the background is balanced by the potentiometer R_3 . The output voltage of the transformer is fed to an AC amplifier and then to the data-acquisition system through an integrating RC circuit ($R = 0.2 \text{ M}\Omega$, $C = 2 \mu\text{F}$).

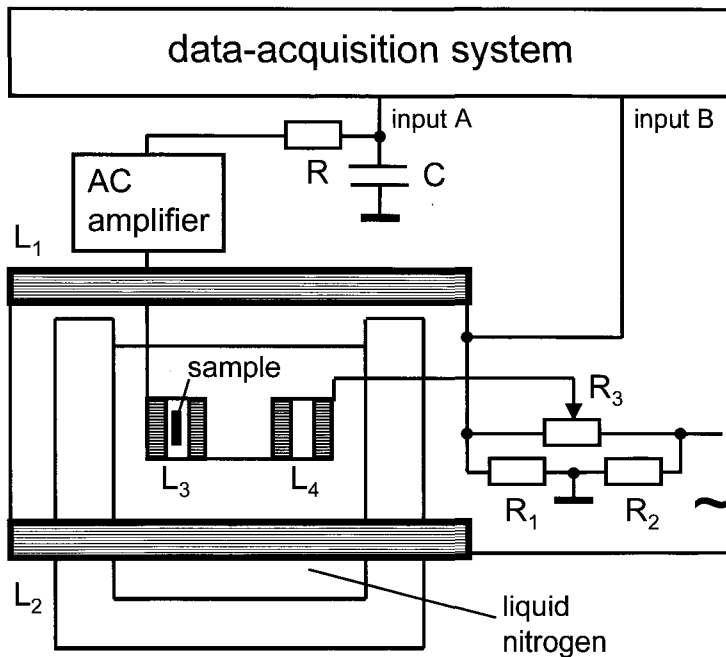


Fig. 8. Diagram of the setup for observing magnetization curves of a superconductor.

With a superconducting sample inside one of the secondary coils, the magnetic flux through it decreases. A voltage therefore appears at the output of the differential transformer. The integrating circuit provides a voltage proportional to the magnetization of the sample M . *DataStudio* displays the magnetization curve $M(B_0)$. The magnetic field produced by

the Helmholtz coils can be calculated or measured by a small probe coil or by a Hall probe. In our case, the maximum magnetic field amounts to 20 mT. For the measurements, a ceramic YBCO tablet is broken into pieces and then sealed in a glass ampoule. The magnetization curves are observed under various amplitudes of the magnetic field. Below the first critical field, the $M(B_0)$ dependence is linear. At higher fields, it becomes nonlinear and hysteretic. Using a small piece of a ferromagnet, it is easy to show that the magnetization in a superconductor is opposite to that in a ferromagnet. The nonlinearity in the magnetization curve is also seen from harmonics in the output voltage of the transformer caused by the sample. For this purpose, the Helmholtz coils are fed by a regulated DC current and a small AC component from a low-frequency oscillator. The *Fast Fourier transform* tool performs the spectral analysis of the output voltage of the differential transformer.

Magnetic susceptibility versus external magnetic field

The influence of external magnetic fields on the magnetic susceptibility of a superconductor is studied by the well-known oscillator technique. The resonance frequency of an LC circuit increases in the presence of a superconducting sample inside or near the inductor. The LC circuit is connected to the X input of an oscilloscope. The oscilloscope, Kenwood model CS-4025, has an output terminal of one channel providing a gain up to 100. The amplified voltage is fed to the LC circuit through a 100-k Ω variable resistor (Fig. 9). Owing to this positive feedback, continuous oscillations occur in the LC circuit. Their frequency is nearly 40 kHz. Changes in the frequency reflect changes in the magnetic susceptibility of the sample. This technique is very sensitive and suitable for measurements in external magnetic fields.

To simplify the experiment, it is conducted with an YBCO sample immersed in liquid nitrogen. The inductor and the sample are positioned in a Dewar flask filled with liquid nitrogen. Helmholtz coils 14 cm in diameter, each containing 320 turns, produce an external DC magnetic field. A digital frequency meter measures the oscillation frequency. The relative change in the frequency due to a sample depends on the volume inside the inductor occupied by the sample. In our case, this change is approximately 5%, while the instability of the frequency is less than 0.01%. Hysteresis in the magnetic susceptibility of the sample is evident (Fig. 10). This dependence was obtained under zero-field cooling of the sample. In a 9-mT field, the susceptibility decreases by approximately 20%.

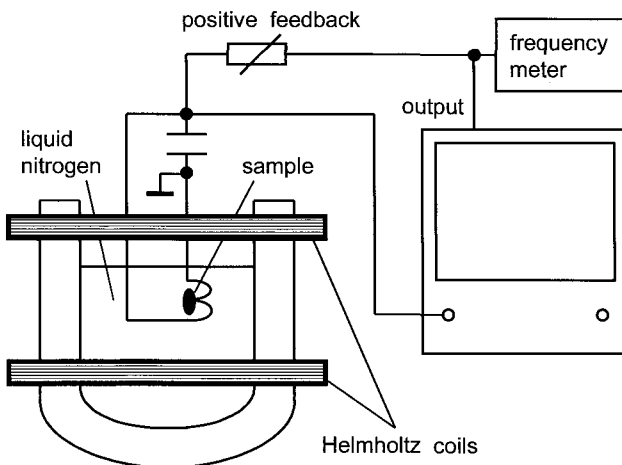


Fig. 9. Observation of the influence of an external DC magnetic field on the magnetic susceptibility of a superconductor.

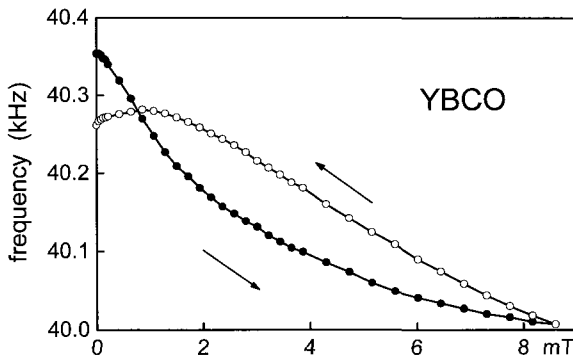


Fig. 10. Oscillation frequency versus external field for an YBCO sample.

Transition curve

In this experiment, a number of pieces of the same superconducting tape, 0.5 to 1 cm long, are placed into a glass container, 1 cm in diameter and 2 cm in height, together with a small platinum resistance thermometer ($100\ \Omega$ at 0°C) inside. A differential transformer serves for measuring the magnetic susceptibility of the sample (Fig. 11). A 200-turn coil, 21 cm in diameter (PASCO, EM-6711), forms the primary winding of the transformer fed by the *Signal generator*. The frequency of the current feeding the primary winding may be chosen in a wide range, from

several tens to several hundreds of hertz. As a rule, we perform the measurements at 90 Hz, and the amplitude of the AC magnetic field is 0.2 mT. A second similar coil allows one to study the influence of external DC magnetic fields on the transition curve.

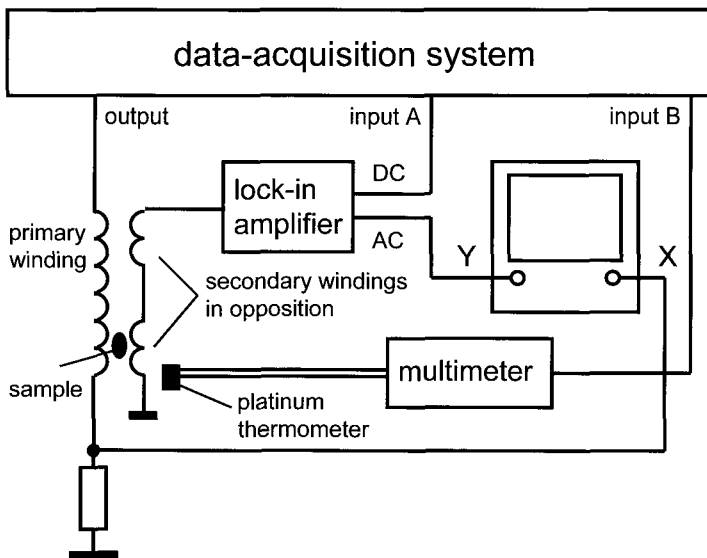


Fig. 11. Diagram of the setup with a differential transformer.

A glass Dewar flask with liquid nitrogen rests on a laboratory jack inside the coils and can be raised and lowered (Fig. 12). Two similar secondary coils positioned inside the flask are connected in opposition, so that in the absence of a sample the output voltage of the differential transformer is zero. Each secondary coil, 2 cm in diameter and 2 cm in height, contains 500 turns.

With a superconducting sample inside one of the secondary coils, the magnetic flux through it decreases. A voltage therefore appears at the output of the differential transformer. This voltage is proportional to the magnetic susceptibility of the sample and serves for recording the phase transition from the superconducting to the normal state. A lock-in amplifier, PAR model 124A, measures this voltage and provides a DC output voltage for the data-acquisition system and an amplified AC voltage for the Y input of an oscilloscope. A voltage proportional to the current in the primary coil serves as the reference for the lock-in amplifier and the signal for the X input.

The resistance of the platinum thermometer is measured by a Keithley 177 model multimeter. The output voltage of the multimeter

proceeds to the second input of the data-acquisition system and then is translated into temperature. After cooling the secondary coils and the sample in the liquid nitrogen, the Dewar flask is lowered, so that the sample appears above the liquid. Without a sample, the secondary coils are positioned to minimize the output voltage of the differential transformer. Then the sample is put into one of the secondary coils. The DC output voltage of the lock-in amplifier is displayed by the data-acquisition system versus temperature when the sample starts to warm up. The heating rate depends on the distance between the sample and the level of liquid nitrogen and on the temperature of the sample.

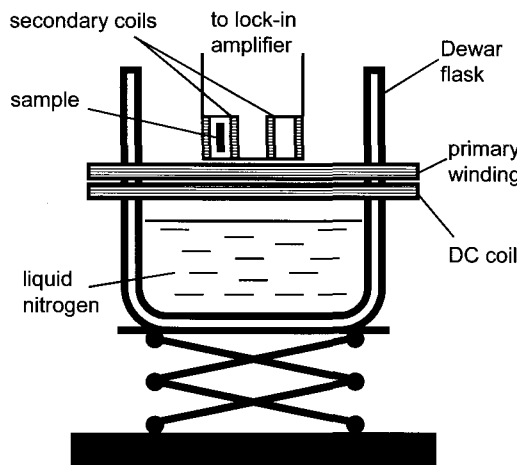


Fig. 12. Arrangement for measuring the magnetic susceptibility versus temperature.

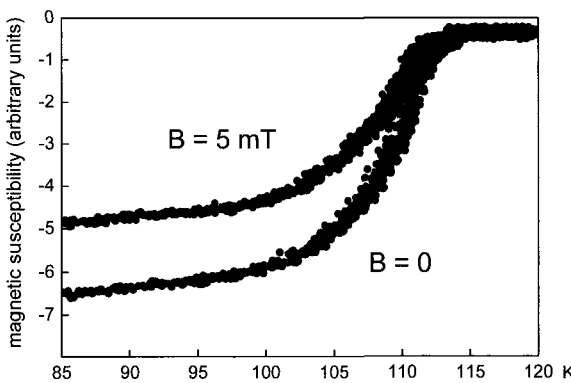


Fig. 13. Transition curves of BSCCO-2223/Ag sample obtained by measurements of its magnetic susceptibility.

To ensure good thermal equilibration between the sample and the thermometer, the heating rate should not exceed $2 \text{ K} \cdot \text{min}^{-1}$. The *Sample rate* is set at 1 or 2 Hz. The temperature dependence of the magnetic susceptibility of the sample (Fig. 13) clearly shows the phase transition from the superconducting to the normal state. Above the critical temperature, the output voltage of the differential transformer becomes zero. Due to the low frequency of the magnetic field and small dimensions of the conducting pieces of the sample, eddy currents in them are too small to influence the results. In an external DC magnetic field, the magnetic susceptibility of the sample decreases. In the experiment, a DC current in the second large coil produces this field. The maximum current allowed for the coil is 2 A, and the corresponding magnetic field is about 5 mT.

Diamagnetism of superconductors

In this demonstration (Kraftmakher 2004e), pieces of a superconducting tape, 2 to 2.5 cm long, are placed into a plastic cup, which can be filled with liquid nitrogen. A differential transformer with an E-shaped core (PASCO, SF-8615) senses the magnetic susceptibility of the sample (Fig. 14). Two 800-turn coils L_1 and L_2 (SF-8611) form the primary winding of the transformer fed by a function generator. A 3200-turn coil L_3 (SF-8613) constitutes the secondary winding of the transformer. The coils L_1 and L_2 fed by the *Signal generator* generate opposite magnetic fluxes through the coil L_3 . Without a sample or above its critical temperature, the output voltage of the transformer is thus zero.

The *Scope* displays the output voltage of the differential transformer versus a voltage across a $1\text{-}\Omega$ resistor placed in series with the primary windings. An ellipse is seen on the screen. The *Scope* serves also for adjusting the transformer before the measurements. This is done by arranging the primary coils. The frequency of the current in the primary windings is 30 Hz. When a superconducting sample is placed in one arm of the magnetic core, the magnetic flux through this arm decreases, and a voltage appears at the output of the differential transformer. This voltage is proportional to the magnetic susceptibility of the sample. The students observe the phase transition from the superconducting to the normal state after evaporation of the liquid nitrogen from the plastic cup. A small piece of a ferromagnet is used to show that the superconducting sample is diamagnetic.

The demonstration is possible without a data-acquisition system. An YBCO tablet is wrapped by a metal foil and placed in a plastic cup

positioned in one arm of the differential transformer. Its primary coils are connected to a function generator. The output voltage of the transformer is seen on the screen of an oscilloscope.

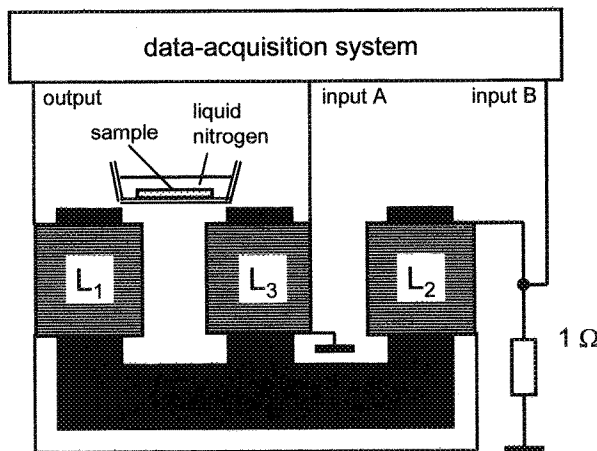
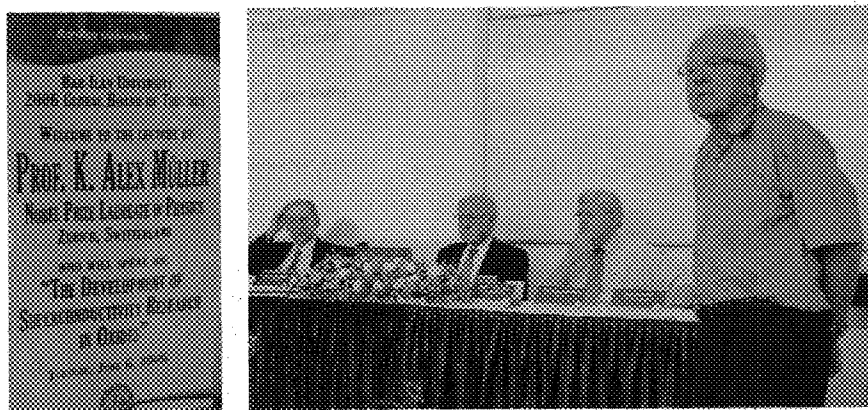


Fig. 14. Setup for demonstrating diamagnetic properties of superconductors.



It remains to say that Professor Müller is Doctor *honoris causa* of Bar-Ilan University. A meeting with the Nobel laureate recently took place at the Physics Department. From left to right: Professor Moshe Kaveh, President; Professor K. Alex Müller; Professor Yosef Yeshurun, Rector; Professor Moshe Gitterman is introducing the Nobel laureate.